(2)

DOT/FAA/CT-87/37

FAA Technical Center
Atlantic City International Airport
N.J. 08405

De-Icing of Aircraft Turbine Engine Inlets

H.A. Rosenthal
D.O. Nelepovitz
H.M. Rockholt

Rohr Industries, Inc.
Chula Vista, California

June 1988

Final Report

U.S. Department of Transportation
Federal Aviation Administration

NOTICE

This document is disseminated under the sponsorship of the Department of Transportation in the interest of information exchange. The United States Government assumes no liability for the contents or use thereof.

The United States Government does not endorse products or manufacturers. Trade or manufacturers' names appear herein solely because they are considered essential to the object of this report.

Technical Report Documentation Page

1. Report No.	2. Government Accession No.	3. Recipient's Catalog No.
DOT/FAA/CT-87/37		

4. Title and Subtitle	5. Report Date
De-Icing of Aircraft Turbine Engine Inlets	June 1988
	6. Performing Organization Code
	8. Performing Organization Report No.
7. Author(s)	
H. Rosenthal, D. Nelepovitz, H. Rockholt	
9. Performing Organization Name and Address	10. Work Unit No. (TRAIS)
Rohr Industries, Inc. P.O. Box 0878 Chula Vista, California 92012-0878	11. Contract or Grant No. DTFA03-86-C-0050
	13. Type of Report and Period Covered
12. Sponsoring Agency Name and Address	Final October 1986-June 1988
U.S. Department of Transportation Federal Aviation Administration Technical Center Atlantic City, International Airport, N.J. 08405	14. Sponsoring Agency Code

15. Supplementary Notes

Flight Safety Research Branch, ACT-340
Gary Frings, Project Manager/Contracting Officer's Technical Representative

16. Abstract

This document presents the results of an FAA investigation to determine the effects of using de-icing,as opposed to anti-icing,in aircraft turbine engine inlets. A literature search was conducted. Ice protection equipment technology was assessed.

This report describes the icing/de-icing process,discusses de-ice system operation and performance and ice detector characteristics,and presents a method for determining the effects of the de-icing process on the turbine engine and its associated induction system.

17. Key Words	18. Distribution Statement
Aircraft Icing, De-Icing Systems, Ice Detectors, Anti-Icing	Document is available to the U.S. public through the National Technical Information Service, Springfield, Virginia 22161

19. Security Classif. (of this report)	20. Security Classif. (of this page)	21. No. of Pages	22. Price
Unclassified	Unclassified		

Form DOT F 1700.7 (8-72) Reproduction of completed page authorized

PREFACE

Major contributors to this study were:

— Mr. Steve Clark, Ms. Sue Downs, Dr. Graham Lewis and Mr. Ian Stewart--Rolls-Royce, plc;
-- Dr. Glen Zumwalt--Wichita State University;
-- Mr. Al Weaver--Pratt & Whitney, Inc.; and
— Dr. Bonnie Granzow--Rohr Industries, Inc. (writing services)

TABLE OF CONTENTS

LIST OF ILLUSTRATIONS

LIST OF TABLES

Table — Page

EXECUTIVE SUMMARY

Turbine-engined aircraft are faced with potential problems from the buildup of ice on the inlet ducts of the engines. Such icing could restrict the airflow through the engine, affect engine performance and possibly cause engine malfunction. Furthermore, accreted ice, if dislodged, could enter the engine and seriously damage it.

Turbine-engined aircraft traditionally have used anti-iced air inlets for flight into known icing conditions. These systems use large amounts of engine compressor bleed air or electricity, which may result in an attendant fuel consumption penalty. This penalty may be minimized if de-iced, rather than anti-iced inlets are used.

Advances in de-icing technology have led the aircraft industry to consider that inlets on some new engines be de-iced, rather than anti-iced. For this reason, the Federal Aviation Administration Technical Center is examining de-icing technology, the impact of de-icing system operation on the turbine engine, and the potential for increased use of de-icing systems on more aircraft.

This report details the results of an investigation into de-icing systems. The conclusions are:

—Due to energy considerations, a demand to use de-iced inlets is expected to increase in the mid-1990s.

—Three new de-icing systems—electromagnetic impulse, electromagnetic expulsive and pneumatic impulse have been shown to be feasible.

—De-icing systems must be evaluated to determine the thickness and shape of ice they cause to be shed.

—Damage tolerance levels can be established and included in the specifications for the design of de-icing systems.

INTRODUCTION

OBJECTIVE.

Recent research into new aircraft ice protection technologies offers the possibility that de-icing systems may be used on aircraft turbine engine inlets that would otherwise be equipped with anti-icing systems. The objective of this project was to investigate the de-icing technology available, and that being developed and to determine the effects of these de-icing systems on the engines.

To evaluate the effects of de-icing systems on the engines, this study aimed to: 1) determine the amount of inlet ice that accretes between de-icing cycles; 2) identify analytical and/or empirical methods for determining the size, amount and path of ice shed during de-icing of an inlet lip; and 3) determine what type of engine or inlet damage can be caused by ice shed from the inlet.

BACKGROUND.

Anti-icing systems prevent ice from forming on a surface, whereas de-icing systems dislodge ice that has been allowed to form. One possible advantage of de-icing over anti-icing is the potential for reduced specific fuel consumption (SFC). To prevent the formation of ice, an anti-icing system must be continually operated in icing conditions and, as a result, requires a large energy input. This energy is derived by consuming fuel, thereby creating a significant SFC penalty. This SFC penalty is expected to be even more severe in the next generation of turbine engines, which, because of their high-bypass design, will have a decreased airflow to the core engine and, in turn, less hot compressor bleed air available for heating aircraft surfaces. A de-icing system, on the other hand, uses much less energy because the system need not be operated continually in icing conditions, but only at intervals, just enough to keep ice from building up beyond tolerable levels.

A major concern when applying de-icing systems to turbine engine inlets is the effect of ice shed into the engine. Shed ice could impact various engine components such as fan blades, guide vanes, acoustic panels, etc. Ice accreted on inlet surfaces between de-icing cycles may also cause some airflow disruption, thereby affecting engine performance. These concerns are addressed and recommendations are made to minimize these effects.

Some aircraft with de-icing systems are equipped with particle separators to reduce or eliminate engine ingestion of ice shed from the inlet. This report addresses de-icing both with and without particle separators.

DE-ICING TECHNOLOGY STATUS

OVERVIEW.

This section provides a summary of aircraft ice protection, comparing evaporative anti-icing, "running wet" anti-icing, and de-icing. It then details the current status of aircraft de-icing technology, both that in service on aircraft and that in development. Material covered in this section was gathered from survey questionnaires sent to airframe, engine, ice detection and de-icing system manufacturers. Respondents to the survey are listed in Table 2-1. Table 2-2 relates the various types of ice protection to the engines on which they are used.

The engine/nacelle installation in Figure 2-1 illustrates the relationship between the forward parts of the engine and the lip of the engine inlet duct where ice accretion can occur during flight through icing conditions. In order to avoid intolerable amounts of inlet ice buildup, some type of ice protection is used. Completely evaporative anti-icing causes water impinging on the engine inlet lip to evaporate, thereby preventing formation of ice. "Running wet" anti-icing systems do not necessarily supply enough heat to cause evaporation of all impinging water, but are able to keep the water above the freezing point. In some of these systems the water may run back to unheated regions and freeze there.

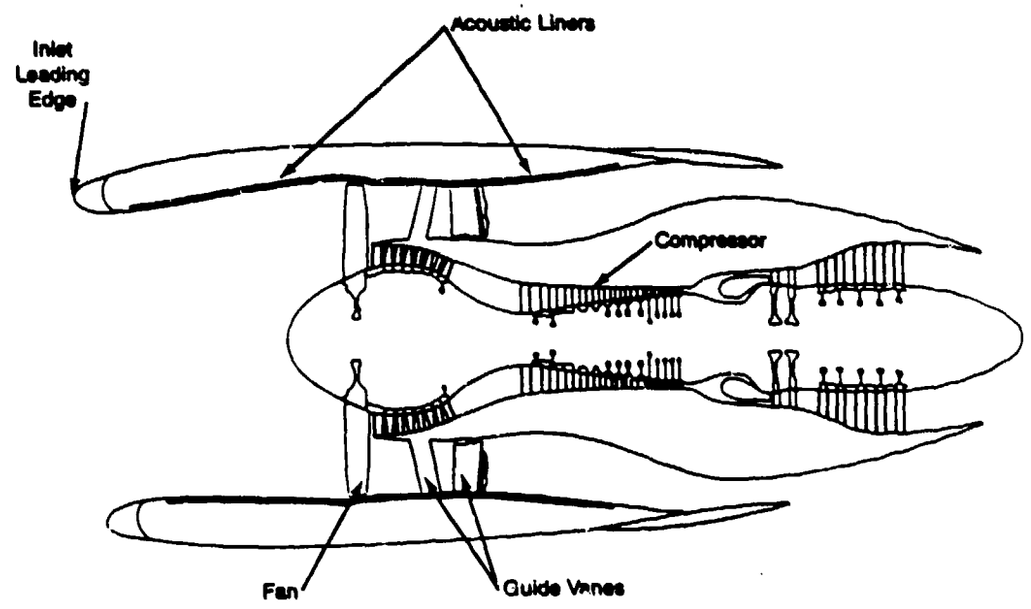

Figure 2-1. Schematic of Engine/Nacelle Installation—This schematic illustrates the spatial relationships between the inlet leading edge, where ice accretion can occur, and components of the engine/inlet that might be subject to damage from ice dislodged from the inlet leading edge.

Table 2-1. Respondees to De-Icing Technology Status Questionnaire

AIRFRAME MANUFACTURERS

Avions Marcel Dessault-Breguet Aviation (France)
Beech Aircraft Corp. (United States)
Boeing Commercial Airplane Co. (United States)
British Aerospace plc (Great Britain)
Cessna Aircraft Co. (United States)
DeHavilland Canada, Inc. (Canada)
Douglas Aircraft Co. (United States)
Fairchild Aircraft Corp. (United States)
Lockheed-California Co. (United States)

ENGINE MANUFACTURERS

Avco Lycoming Textron (United States)
Pratt & Whitney Canada (Canada)
Rolls-Royce plc (Great Britain)

DE-ICING SYSTEM MANUFACTURERS

AEG-Aktiengesellschaft,
Space & New Technologies Div. (Germany)
BF Goodrich (United States)
Innovative Dynamics (United States)
Lucas Aerospace Ltd. (Great Britain)
Simmonds-Precision (United States)
TKS Aircraft De-Icing Ltd. (Great Britain)

ICE DETECTOR MANUFACTURERS

Dataproducts N.E. (United States)
Lucas Aerospace Ltd. (Great Britain)
Rosemount, Inc. (United States)
Simmonds-Precision (United States)
Vibro-meter Corp. (United States)

Table 2-2. Ice Protection Systems Currently Used on Aircraft *

Ice Protection System	Engine		Aircraft	Company
Anti-icing— Hot compressor air	CF700	Turbofan	Falcon 20	Avions Marcel Dassault
	TFE731-2	Turbofan	Falcon 10/100	Avions Marcel Dassault
	TFE731-3	Turbofan	Falcon 50	Avions Marcel Dassault
	ATF3-6A	Turbofan	Falcon 200	Avions Marcel Dassault
	ATF3-6	Turbofan	HU25A	Avions Marcel Dassault
	TFE731-5A	Turbofan	Falcon 900	Avions Marcel Dassault
	JT3D	Turbojet	707	Boeing
	JT8D	Turbofan	727	Boeing
	JT8D	Turbofan	737	Boeing
	JT9D/CF6/RB211-524	Turbofan	747	Boeing
	RB211-535/PW2037	Turbofan	757	Boeing
	JT9D/CF6	Turbofan	767	Boeing
	ATF502	Turbofan	BAe 146	British Aerospace
	TFE731-3B	Turbofan	650	Cessna
	TPE331-8-403S	Turbofan	441	Cessna
	CT64-820-4	Turbojet	DHC-5 Buffalo	DeHavilland Canada
	CFM56	Turbofan	DC-8-70	Douglas Aircraft Co.
	JT8D-217	Turbofan	MD-80	Douglas Aircraft Co.
	JT8D-219	Turbofan	MD-83	Douglas Aircraft Co.
	CF6-50-C2	Turbofan	KC-10	Douglas Aircraft Co.
	CF6-50-C2	Turbofan	DC-10-30	Douglas Aircraft Co.
	CF6-6K2	Turbofan	DC-10-10	Douglas Aircraft Co.
	JT9D-20J	Turbofan	DC-10-40	Douglas Aircraft Co.
	RB211	Turbofan	L-1011	Lockheed
	TF-34	Turbofan	S-3	Lockheed
Anti-icing— Hot compressor air and electric heating	JT15D-1, D-1A, D-1B	Turbojet	500/501	Cessna
	JT15D-4	Turbojet	500/551	Cessna
Anti-icing Hot compressor air and hot oil	JT15D-4B	Turbojet	S550	Cessna
Anti-icing— Hot exhaust gas, inertial particle separator and ¼" mesh protective screen	PT6A-21	Turboprop	King Air Model C90A	Beech Aircraft Corp.
	PT6A-42	Turboprop	King Air Model 200	Beech Aircraft Corp.
	PT6A-60A	Turboprop	King Air Model 300	Beech Aircraft Corp.
	PT6A-65B	Turboprop	Model 1900 Commuter	Beech Aircraft Corp.
	PT6A-42	Turboprop	C12 Military Series	Beech Aircraft Corp.
	PT6A-25	Turboprop	T34C (Single Engine)	Beech Aircraft Corp.
Anti-icing— Hot exhaust gas and inertial particle separator	PT6A-112	Turboprop	406/425	Cessna
Anti-icing— Hot exhaust gas	PT6A-45R	Turboprop	Metro IIIA, SA227-PC	Fairchild
	PT6A-60	Turboprop	Merlin IVC SA227-PT	Fairchild
	PT6A-60	Turboprop	Merlin IIID, SA227-TP	Fairchild
De-icing— Hot compressor air	TPE331-3	Turboprop	Metro II, IIA, SA226-TC	Fairchild
	TPE331-11	Turboprop	Metro III SA227-AC	Fairchild
	TPE331-3	Turboprop	Merlin IV, IVA, SA226-AT	Fairchild
	TPE331-11	Turboprop	Merlin IVC, SA227-AT	Fairchild
	TPE311-11	Turboprop	Expediter, SA227-AT	Fairchild
	TPE331-3	Turboprop	Merlin III, SA226-T	Fairchild
	TPE331-3	Turboprop	Merlin IIIA, SA226-T	Fairchild
	TPE331-10	Turboprop	Merlin IIIB, SA226-T(B)	Fairchild
	TPE331-10	Turboprop	Merlin IIIC, SA227-TT	Fairchild
	PT6A-60	Turboprop	Merlin IIID, SA227-TP	Fairchild
De-icing— Electric heating and inertial particle separator	PT6A-27	Turboprop	DHC-6 Twin Otter	DeHavilland Canada
De-icing— Pneumatic boot and inertial particle separator	PT6A-50	Turboprop	DHC-7	DeHavilland Canada
	PW120	Turboprop	DHC-8	DeHavilland Canada
	PW118	Turboprop	EMB-120	Embraer
	PT6A-45	Turboprop	M298	Frakes
Inertial Particle Separator	PT6A-114	Turboprop	208	Cessna

* This table was compiled from the survey responses and, therefore, is by no means complete, in part, because some manufacturers opted not to disclose proprietary information.

In contrast to an anti-icing system, a de-icing system is designed to remove ice that has been allowed to accumulate to some level predetermined to be tolerable to the aircraft and engine. Therefore, de-icing expends much less energy than anti-icing because the system is activated only at regular intervals, with ice buildup allowed between de-icing cycles. The timing of the cycles is a function of the particular system being used and the icing conditions being faced.

ANTI-ICING.

Since the advent of the gas turbine engine, hot bleed air from the engine's high-pressure compressor has been available as a heat source for anti-icing engine inlets. This source can supply enough heat to prevent ice formation throughout most icing conditions for large turbine engine/nacelle installations (Table 2-2).

Three different systems for channeling and directing hot anti-icing air over the backside of the engine inlet leading edge have been developed (Fig. 2-2). In the double-wall system, hot air circulates through a duct formed between the bulkhead and an inner leading edge wall and flows through holes in the inner wall to heat the outer wall of the inlet leading edge

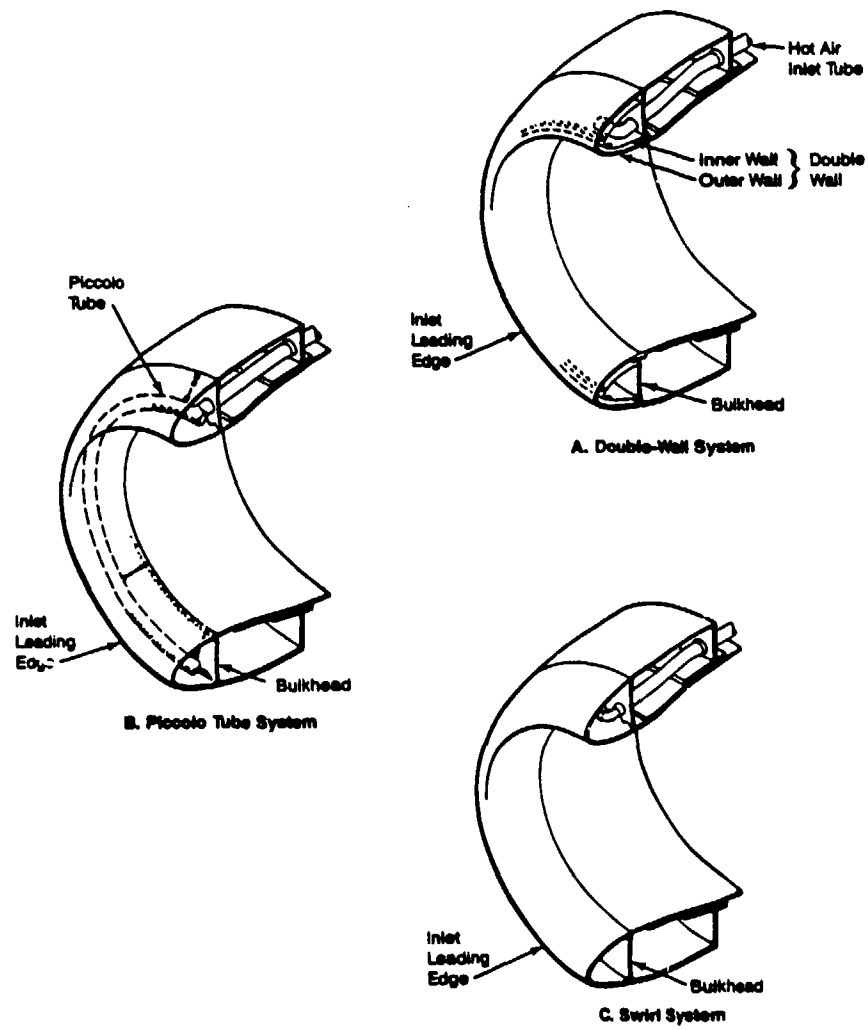

Figure 2-2. Anti-Icing Channeling Systems

(Fig. 2-2A). The piccolo tube system is a modification of the double-wall system in which the inner leading edge wall is omitted and hot air circulates through a tube that extends around the circumference of the inlet. Air exits from holes in the tube to heat the inlet leading edge (Fig. 2-2B). The swirl system is a further simplification in which the circumferential piccolo tube is omitted so that hot air swirls around the circumference of the inlet leading edge in the entire space forward of the bulkhead (Fig. 2-2C).

Very few turboshaft engine installations, such as turboprops, use engine compressor air for inlet anti-icing. Instead, alternative heat sources such as exhaust gas, hot engine oil, electrothermal heater mats, or a combination of these sources are used (Fig. 2-3). In extreme icing conditions, some of the water may run back to unheated regions of the inlet and freeze there. This condition is called "running wet." Running-wet systems use low amounts of energy compared to completely evaporative anti-icing systems. This is why running-wet systems are preferred in engines that cannot afford to expend a lot of energy on ice protection.

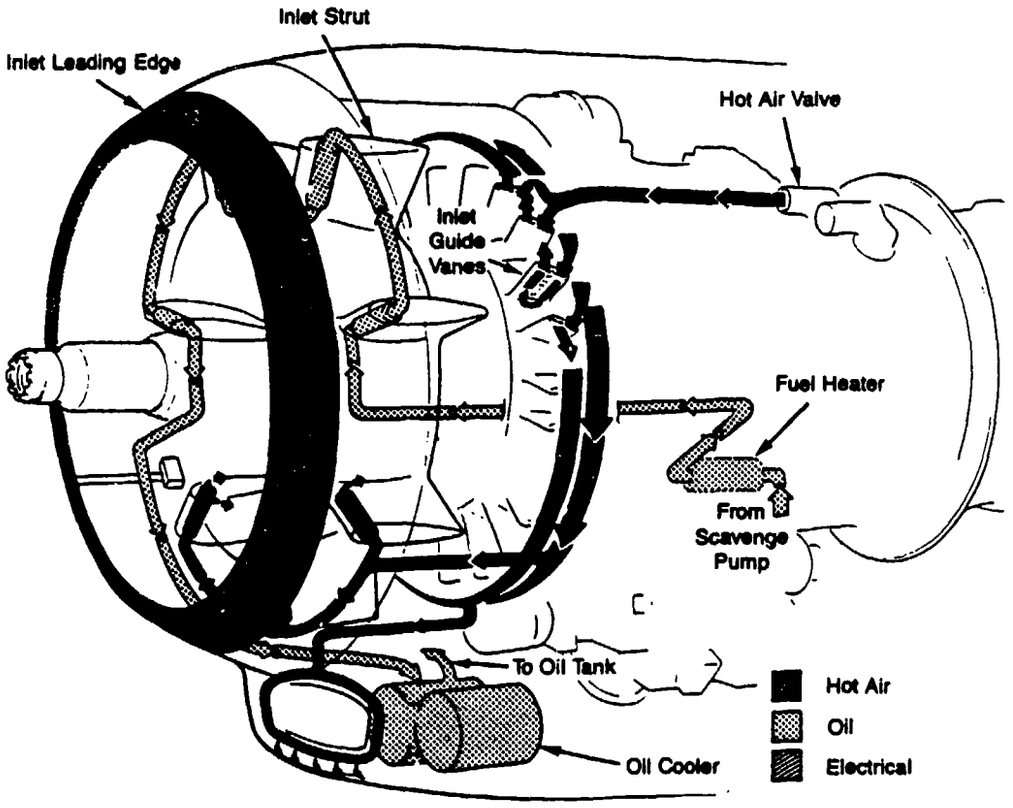

Figure 2-3. Combination of Hot Air, Oil and Electrical Ice Protection in a Turbine Installation

In some running-wet systems, water channels are designed into the inlet's surface to divert water overboard or away from the engine. This type of diversion keeps the water from collecting on and freezing to the inlet leading edge. Not all running-wet systems require water channels; the design of some engines incorporates inlet air bypass ducts that channel a certain portion of the inlet air away from the engine. These bypass ducts can be modified to also serve as particle separators that divert foreign objects such as birds and ice away from the engine (Fig. 2–4). These same bypass ducts can also help channel water away from the inlet's leading edge.

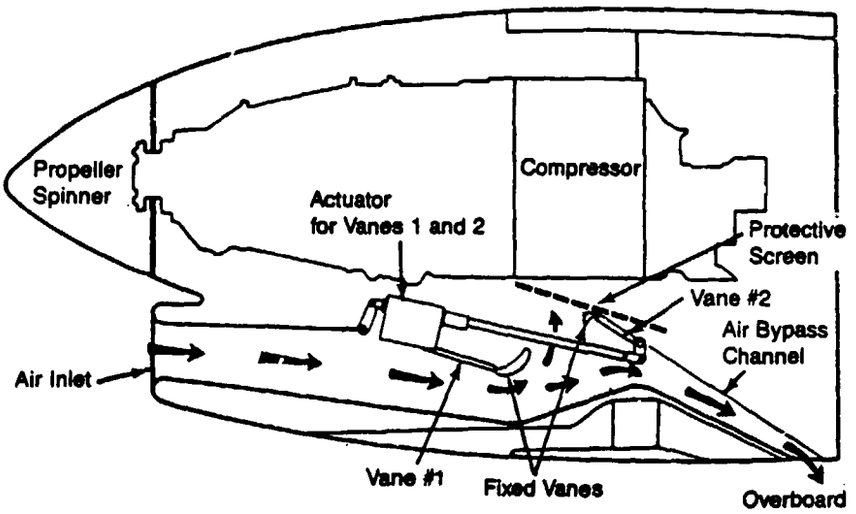

Position of Vanes and Airflow for Icing Conditions

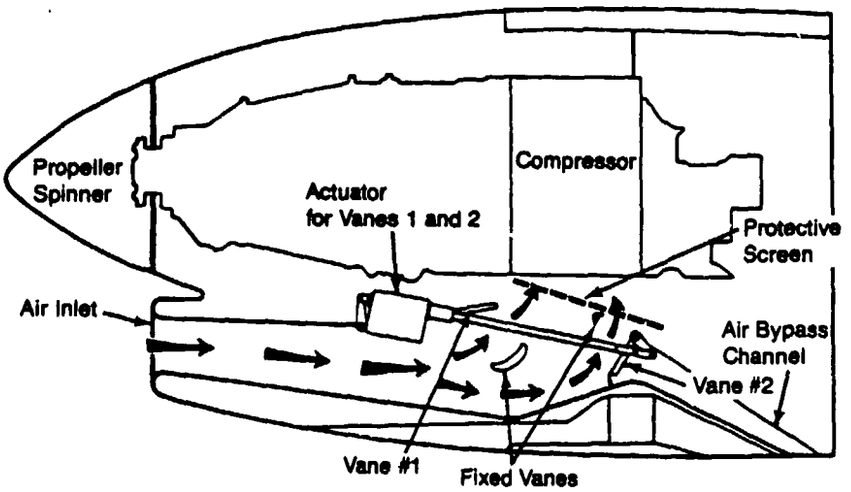

Position of Vanes and Airflow for Non-Icing Conditions

Figure 2-4. Turboprop Inertial Particle Separator—During icing conditions some airflow is diverted downward away from engine, carrying the heavier-than-air ice particles with it.

In aircraft where water running back and freezing on unheated regions of the inlet creates an unacceptable risk, the same energy sources used for anti-icing water-impingement areas, such as the inlet leading edge, can be used for de-icing the areas further aft where water collects and freezes. This ice protection technique is another way to reduce energy consumption compared to anti-icing all regions.

Some propeller-driven aircraft still use a system consisting of air heated by an exhaust manifold for anti-icing.

DE-ICING.
Engine inlet de-icing systems have been developed for aircraft in which energy consumption must be kept to a minimum. This section describes the de-icing systems currently in use (electrothermal mats and pnuematic boots) and those under development (pneumatic impulse, piezoelectric vibration, electro-expulsive and electromagnetic impulse de-icing). Of the latter, electromagnetic de-icing (EIDI) appears to be the most mature at this time due to the relatively high level of research and development associated with it. Research on EIDI, in which Rohr and Rolls-Royce have participated extensively, is detailed in Appendix B.

For many de-icing applications, ice ingestion is not tolerable and particle separators have become an integral part of these de-icing systems. In those cases in which particle separators are not used, engine tolerance to ice ingestion must be analyzed and assurances made that ice ingestion does not adversely affect safe engine operation.

A related emerging technology—that of improved ice detectors—is anticipated to advance effective and safe de-icing operations. Current research is aimed at developing ice sensors as part of an automated ice detection and de-icing actuator system.

PNEUMATIC BOOTS. Pneumatic boots, currently the most common mechanical systems used for de-icing, are the most widely used means of wing de-icing for general aviation aircraft. They are also used for engine inlet de-icing in several turboprop commuter aircraft (Table 2-2).

A pneumatic boot consists of an inflatable bladder bonded to the surface that requires ice protection (Fig. 2-5 and Ref. 2-1). During operation, pressurized air is forced into the bladder causing it to expand with a surface deflection rate of approximately 0.35 in/sec. This expansion breaks the ice/ bladder bond and fractures accreted ice into small pieces. To promote the breaking of the ice/bladder bond, an ice adhesion reduction agent is often applied to the bladders before each flight.

Due to the deformation imparted to the wing airfoil or inlet leading edge during the activated phase of a de-icing cycle, pneumatic boots are limited to low- and mid-velocity applications (up to Mach 0.5). The pneumatic boot usually requires a vacuum system to keep the bladders flat when not in use, thereby preventing an irregular aerodynamic surface between de-icing inflations.

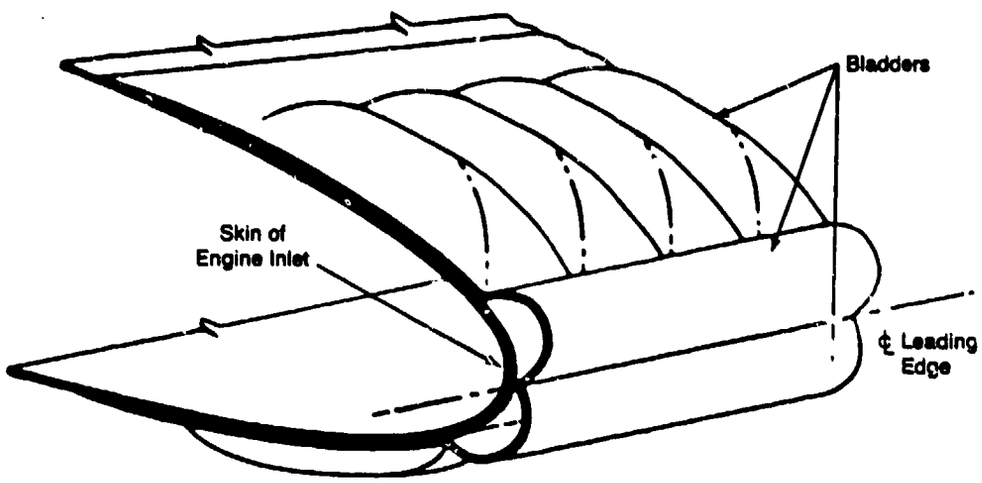

Figure 2-5. Schematic Cross-Section of a Pneumatic Boot De-Icer (Inflated) as Installed on an Engine Inlet

As with many de-icing systems, there is a minimum ice thickness at which pneumatic boots become effective. This is 0.125 inch for current pneumatic boots, but the ice must be a contiguous accretion. Pneumatic boots are optimally effective over an ice thickness range of one-eighth to one-quarter inch. As with most mechanical de-icing systems, rime ice (defined in Appendix A) on the upper and lower airfoil or on the inlet surface will remain attached longer than leading edge ice. Rime ice accretes slowly and can usually be shed before it becomes excessively large and creates an aerodynamic problem.

The size of ice fragments shed by a pneumatic boot is determined by the on/off cycle time and icing conditions. Testing and previous experience with similar engines are taken into consideration and used in evaluating a new application. Many pneumatic boot systems are used in conjunction with inertial particle separators to minimize ice ingestion by the engine. Whether or not a particle separator is required depends on the ice damage tolerance of the engine.

Improvements in the means for retarding erosion of pneumatic boots have resulted in a significant increase in intervals between boot replacements—from 10,000 flight hours in 1950 to 20,000 flight hours in 1980.

Many turboprop aircraft use freezing point depressant (FPD) fluids in conjunction with pneumatic boots for de-icing. These can be applied externally to propeller blades and wings, either manually during ground servicing or in flight by transpiring the FPD through porous external surfaces. In-flight transpiration of FPD is not used, however, in turboprop aircraft where engine bleed air is used to supply cabin air. This limitation avoids the possibility of accidentally contaminating bleed air with FPD which could produce harmful vapors in the cabin.

ELECTRIC HEATERS. Electrothermal de-icing systems are typically used in aircraft where hot-air anti-icing systems are not feasible. Hot air or hot fluid systems have inherently slow thermal responses and may therefore be unsuitable for de-icing. Electrical resistance heaters, however, can provide the rapid heating needed. De-icing cycles can be timed so that little or no runback occurs between heat-on periods.

Electrical resistance heaters consist of mats of strip conductors embedded in surfaces requiring ice protection by sandwiching the mats between layers of neoprene or glass cloth impregnated with epoxy resin (Fig. 2-6). The mats are protected against water erosion, with a special polyurethane-based coating. On turboprop engines, the engine inlet leading edge, the propeller blades and the propeller spinner may use electrical heating for ice protection. Electrical power is supplied by a generator, and to keep the size and weight of the generator to a minimum, the de-icing electrical loads are cycled between the different ice-protected regions.

During operation of the de-icing system, a thin strip of the leading edge of the inlet is continuously heated to prevent an ice cap from forming on it and to help limit the amount of ice that forms on the areas further aft that are intermittently heated (Fig. 2-6.)

The cycle timing of electrical resistance de-icing systems is adjusted to a schedule predetermined to provide sufficient ice protection for the particular icing conditions encountered. A two-speed cycling system is often

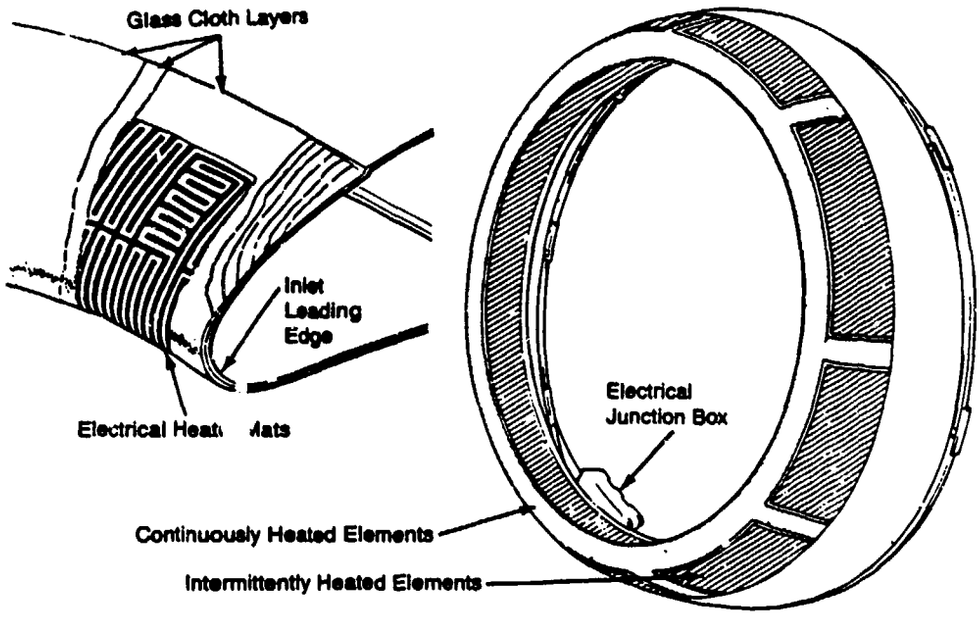

Figure 2-6. Electrical Resistance Heating of Engine Inlet

used—a short-duration cycle at higher air temperatures where the water concentration is usually greater and a long duration cycle in the lower temperature range (Fig. 2-7). The power and timing of the de-icing cycle required for effective de-icing can be estimated, based on analytical methods (Ref. 2-2) and comparisons with other proven de-icing systems, but verification of de-icing effectiveness is checked in icing wind tunnel testing.

The electrical heater type of de-icing system is also used in conjunction with a foreign object bypass duct to prevent most shed ice from being ingested into the engine.

PNEUMATIC IMPULSE. A modification of the pneumatic boot system—the pneumatic impulse de-icing system—is currently under development. This system works essentially the same as the pneumatic boot system, however, instead of expanding slowly, the inflatable bladders are expanded rapidly by high-pressure pulses of air. The surface movement is approximately 0.1 inch in 0.1 second. Because of the shortened times for bladder inflation and, thus, the minimal deformation of airfoil surfaces, this system can be operated on higher speed aircraft than the pneumatic boots. The system currently being developed has a thin titanium sheath covering the flexible boot to enhance durability and reduce erosion.

ELECTROMAGNETIC IMPULSE DE-ICING (EIDI). Electromagnetic impulse de-icing requires no external additions to the aircraft skin. An electric current pulse generated from a capacitor is transmitted through spirally wound, flattened coils made from ribbon wire. The coils are rigidly supported inside the aircraft skin but are separated from it by a gap of approximately 0.1 inch (2.5 mm) (Fig. 2-8). Various coil-mounting configurations are described in Appendix B.

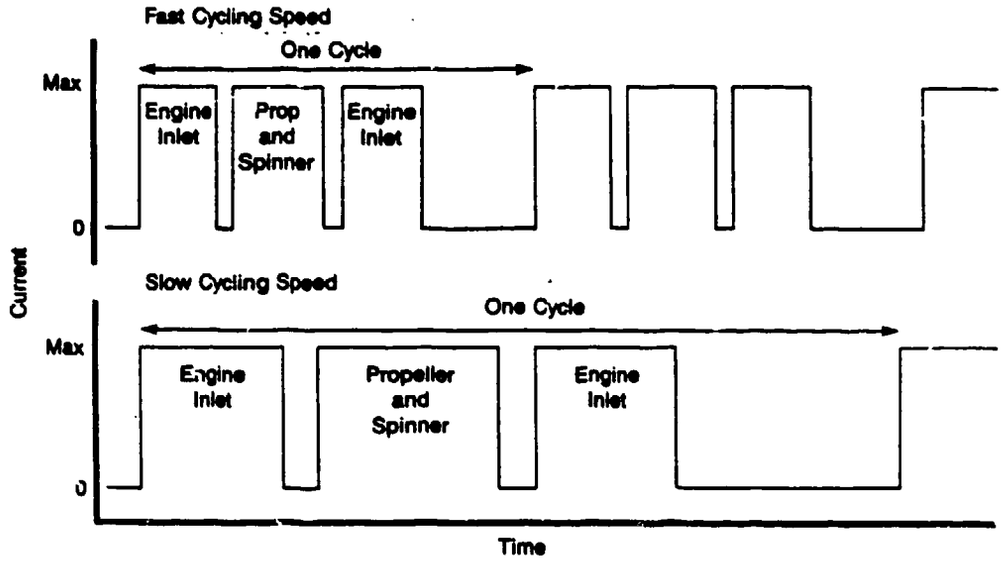

Figure 2-7. De-icing Cycles of Electrical Resistance Heater

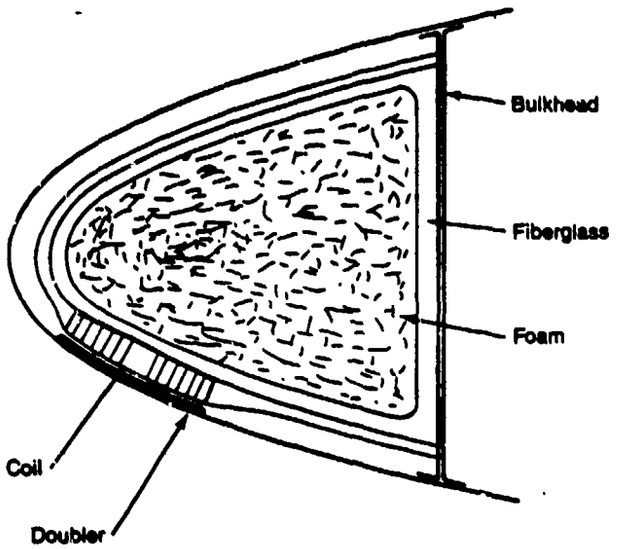

Figure 2-8. Cross-section Through Inlet Leading Edge Showing Bulkhead-Mounted EIDI Coil

The EIDI coil current produces a magnetic field, which induces an eddy current in the thin metal skin (Fig. 2-9). The two currents' fields repel each other. The resultant force causes a low-displacement, high-acceleration movement (0.01 inch per 0.001 second) of the skin adjacent to the coil. This movement shatters the ice and breaks the bond between ice and skin; the ice is then swept away from the surface by aerodynamic forces. This crack/debond/dislodge process usually requires two impulses separated by the recharge time of the capacitators, typically three or four seconds. The power supply is then electrically switched to a coil (or coils) at another location on the engine inlet and the process is repeated. The system cycles back to the original coils before an appreciable amount of ice is accreted.

Connecting wires from capacitor to EIDI coil must be low in resistance and inductance to achieve the fastest impulse response. If the inlet skin thickness is less than the minimum required for adequate conductance of the induced eddy currents, metallic doublers are used to increase conductance (Fig. 2-8). These doublers are usually aluminum discs, slightly larger than the coils, bonded to the skin between the skin and the coil. Metallic doublers are a necessity for non-metallic composite skins.

The energy required for electromagnetic impulse de-icing of an area is about 1 percent of that required for thermal anti-icing of an equivalent area. To achieve this, EIDI design must carefully match the electrical pulse width to the electrical and structural responses of the leading edge. The design procedure is summarized in Ref. 2-3 and explained in detail in Ref. 2-4.

EIDI is currently under development and is being considered for some new engine ice protection designs. Tests so far performed have demonstrated that EIDI is an effective de-icing system. These tests and their results are summarized in Appendix B.

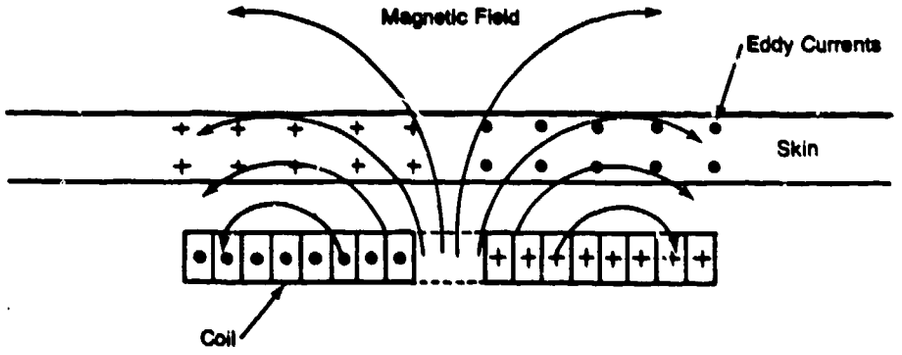

Figure 2-9. Cross-section Through EIDI Coil Showing Coil's Current and Magnetic Field and Resulting Eddy Currents in Skin—Currents flow in a loop in and out of paper plane from "•" to "+".

ELECTROMAGNETIC EXPULSION. Another de-icing system now being tested consists of an electromagnetic expulsive de-icing boot bonded to the inlet surface. The boot consists of an elastomer polyurethane material (thickness 0.02 inch) that has U-shaped ribbon conductors embedded parallel to the boot's surface (Fig. 2-10). A large current from a power storage unit is released through the conductors, creating opposing magnetic fields in adjacent arms of the U-shaped conductors (Fig. 2-11). The magnetic force fields cause the conductors to separate expulsively, forcing the upper expandable surface of the boot to separate from the lower fixed surface of the aircraft.

The boot deflects 0.09 inch in 200 microseconds, creating a G-force in the range of 700-1500 g's. The elastic properties of the boot then quickly collapse it back to a thin layer. The boot's short deflection time makes this system applicable throughout the subsonic and transonic ranges (and possibly into the supersonic range). The energy requirements are 750-1500 joules for a range of 1000-2000 volts (Ref. 2-5), which is effective in removing ice accretion thicknesses of 0.020 - 1.0 inch.

The material from which the boot is made is currently used on several naval aircraft (including the F/A-18) (Ref. 2-6) to provide protection against rain erosion. From this experience, it has been possible to estimate the lifetime of the boots at 10+ years. A particular benefit of this de-icing system is that it is applied externally and therefore easily retrofitted on existing aircraft.

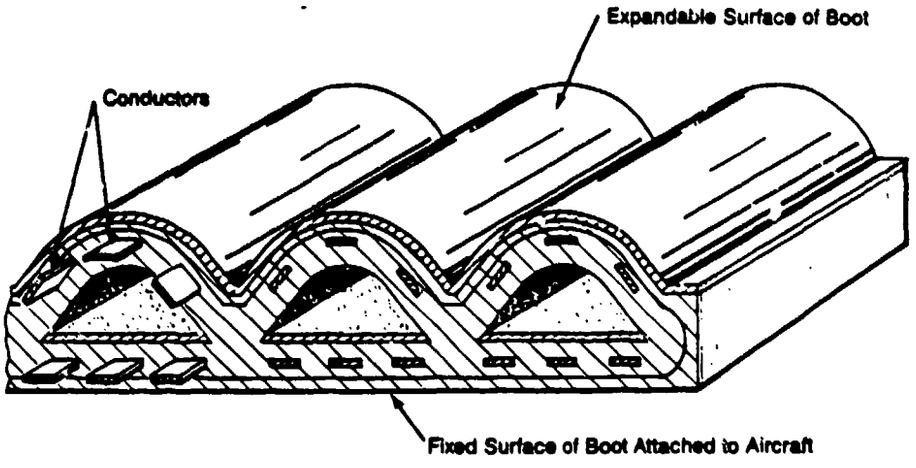

Figure 2-10. Electromagnetic Expulsive De-Icing Boot Shown in Expanded State

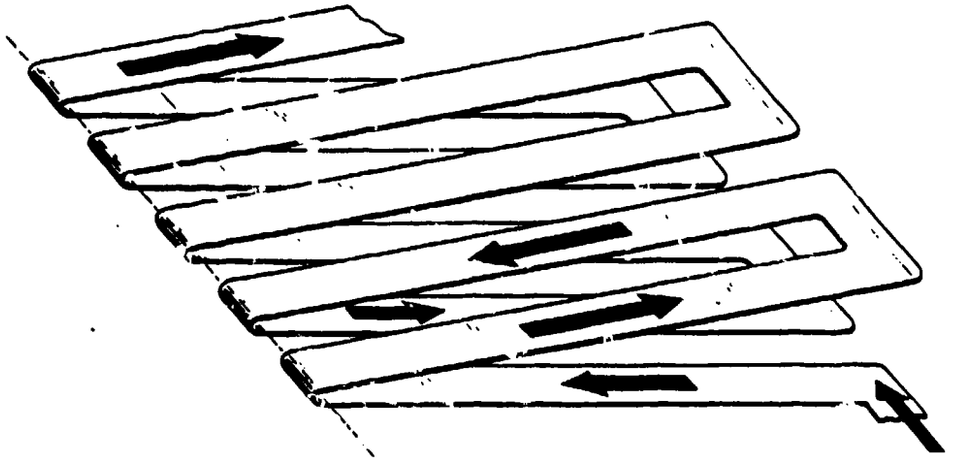

Figure 2-11. Arrangement of Ribbon Conductors in Electromagnetic Expulsive De-Icing Boot—Direction of current flow is indicated by arrows.

HELICOPTERS. Most helicopters do not have an ice removal system that is effective throughout the FAR envelope of icing conditions. As of this time, no U.S.-manufactured civilian helicopters are certified for flight in icing conditions. However, electrothermally heated rotors in conjunction with icing rate sensors permit the operation of some military helicopters in light icing conditions by providing protection for a limited set of icing conditions along with information that helps the helicopter pilot judge the duration of safe flight.

For helicopters, the duration of flight in icing conditions is limited by the icing of the hub and rotor blades; therefore, a good portion of icing research focuses on the rotor and hub, rather than on engine inlet ice protection. The severe limitations on helicopter flights into icing conditions have been a driving force behind current efforts to develop new ice protection technologies, such as ice phobic coatings, mechanical vibrators, microwave emittors, EIDI systems and pneumatic impulse systems These technologies, in some cases, may be adaptable to fixed-wing aircraft as well.

A method of engine inlet ice protection unique to helicoptors is the externally mounted heated inlet screen. Electrical resistance heating of the screen keeps large ice accretions from forming, thereby allowing only very small ice fragments (and resulting water) to pass into the engine inlet. The small ice fragments are further removed by an internal particle separator. These systems typically are not intended for long-duration operation or heavy icing conditions. Other means of helicopter ice protection now in use include electrothermal mats and experimental pneumatic boots for rotor systems (Ref. 2-7).

ICE DETECTION SYSTEMS.

In aircraft without ice detectors, air crews are alerted to icing conditions either by weather advisories or by seeing ice accumulating on their aircraft. Ice detectors currently used on production aircraft (Table 2-3) indicate when ice is forming and on which surfaces. New ice detectors are also being developed to measure ice accretion rate and thickness. Such information will be used either by the air crew or by an automatic electronic controller to adjust the de-icing operation to the icing conditions encountered, thus improving the efficiency of de-icing systems.

These and other improvements being developed, such as increased reliability and self-testing, are expected to further change the role of ice detectors from advisory to controlling. Because icing conditions occur infrequently for most commercial aircraft, an ice detection system must be highly reliable and able to function following long inactive periods. This suggests the need for continual self-testing, which is easily achievable with modern electronics.

Most Ice detectors can be classified into four categories based on how they measure accreted ice—vibrational, electrothermal, pulse-echo, and optical.

VIBRATIONAL. Three types of ice detectors use changes in vibration to sense ice. In one system, a vibrating razor-blade type of probe extends from the surface of the aircraft into the airstream. As ice accretes on the blade,

Table 2-3. Aircraft Equipped with Inlet Ice Detection Systems—All Have Vibrational Type Sensors

Aircraft			
Type	Designation (Manufacturer)	Nationality	Engine Designation (Manufacturer)
Civil	A320 (Airbus)	European	CFM56-5A1 (CFM International) V2500 (International Aero Engine)
Civil	747-400* (Boeing)	U.S.A.	CF6-80C (General Electric) PW4000 (Pratt & Whitney) RB211-524D4D (Rolls-Royce)
Civil	B757 (Boeing)	U.S.A.	PW2037 (Pratt & Whitney) RB211-535C/E4 (Rolls-Royce)
Civil	B767 (Boeing)	U.S.A.	CF6-80C (General Electric) JT9D-7R4 & PW4000 (Pratt & Whitney)
Civil	B-N Turbo Islander (Pilatus Britten-Norman)	UK	250-B17C (Allison)
Civil	Casa CN-235 (Airtech)	Spain	CT7-9C (General Electric)
Civil	CL600/601 (Canadair)	Canadian	600 ALF-502 (Lycoming) 601-CF34 (General Electric)
Civil	Concorde (British Aerospace/Aerospatiale)	European	Olympus 593 MK610 (Rolls-Royce/SNECMA)
Civil	L1011 (Lockheed)	U.S.A.	RB211-22B, RB211-524B (Rolls-Royce)
Civil	Partenavia P68TP (Partenavia)	Italy	250-B17C (Allison)
Civil	SF-340 (Saab-Scania)	Sweden	CT7-5A (General Electric)
Civil	Shorts 330 (Shorts)	UK	Canada PT6A-45R (Pratt & Whitney)
Civil	SIAI SF500TP (SIAI-Marchetti)	Italy	250-B17C (Allison)
Military	B1-B (Rockwell)	U.S.A.	F101-GE-102 (General Electric)
Military	C-130 (Lockheed)	U.S.A.	T56-A-TP (Allison)
Military	F-14 (Grumman)	U.S.A.	TF30 P414A (Pratt & Whitney)
Military	F-15 (McDonnell-Douglas)	U.S.A.	F100-PW-100 (Pratt & Whitney)
Military	F-16 (General Dynamics)	U.S.A.	F100-PW-200 (Pratt & Whitney)
Military	F/A-18 (McDonnell-Douglas)	U.S.A.	F404-GE-400 (General Electric)
Military	MB339 (Aermacchi)	Italy	Viper MK680-43 (Rolls-Royce)
Military	Panavia Tornado (Panavia)	Germany	RB199-34R MK101 (Turbo-Union)
Military	SH-6013 (Sikorsky)	U.S.A.	T700-GE-401 (General Electric)
Military	Super Puma (Aerospatiale)	France	Turbomeca Makila (International Aero Engine)
Military	UH-60 (Sikorsky)	U.S.A.	T700-GE-700 (General Electric)

*Future Aircraft (Not Yet in Service)

the mass of the probe is altered and its resonant frequency changes correspondingly. This frequency change is sensed electronically and transmitted to a cockpit display.

The second type of vibrating device is a coin-shaped, piezoelectric diaphragm mounted flush with the surface of the aircraft (Fig. 2-12). When ice accretes on the diaphragm, its stiffness increases proportionally to the thickness of the ice, causing the diaphragm's natural oscillating frequency to increase sharply. This frequency change is measured by conditioning electronics. A piezoelectric system is also available in a probe configuration.

The third type of vibrating device, currently under development, consists of a piezoelectric film bonded to the inside of a structure such as an inlet (Fig. 2-13). A broad band of vibration frequencies is applied to the structure to elicit its natural resonances. Accreted ice changes the structure's

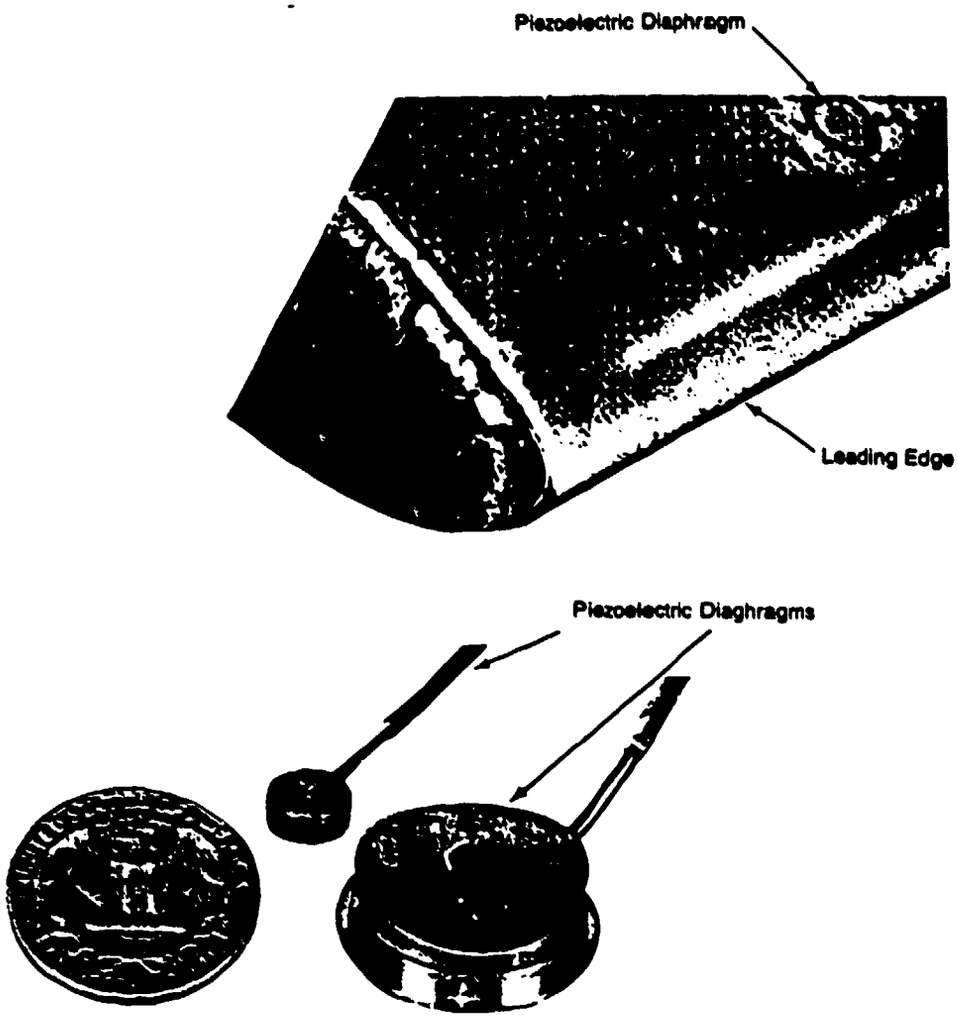

Figure 2-12. Piezoelectric Diaphragm Ice Detector Shown Installed on Aircraft Surface (Top) and Two Variations Shown Next to a Quarter for Size Reference (Bottom)

resonant frequencies. This frequency change is transmitted to a microprocessor that infers ice thickness. This sytem is part of an autonomous ice detection and removal system that has the ability to activate the de-icing process when a predetermined ice thickness is reached.

ELECTROTHERMAL. This type of ice detector operates by sensing changes in electrothermal characteristics of the detector when ice accretes. This detector has a cylindrical probe extending into the airstream with a nickel wire wound around the probe. Electric pulses are continually sent through the wire. When ice accretes on the probe, heat generated in the wire by the electric pulse is absorbed by the ice, and this heat change in the wire is monitored electonically.

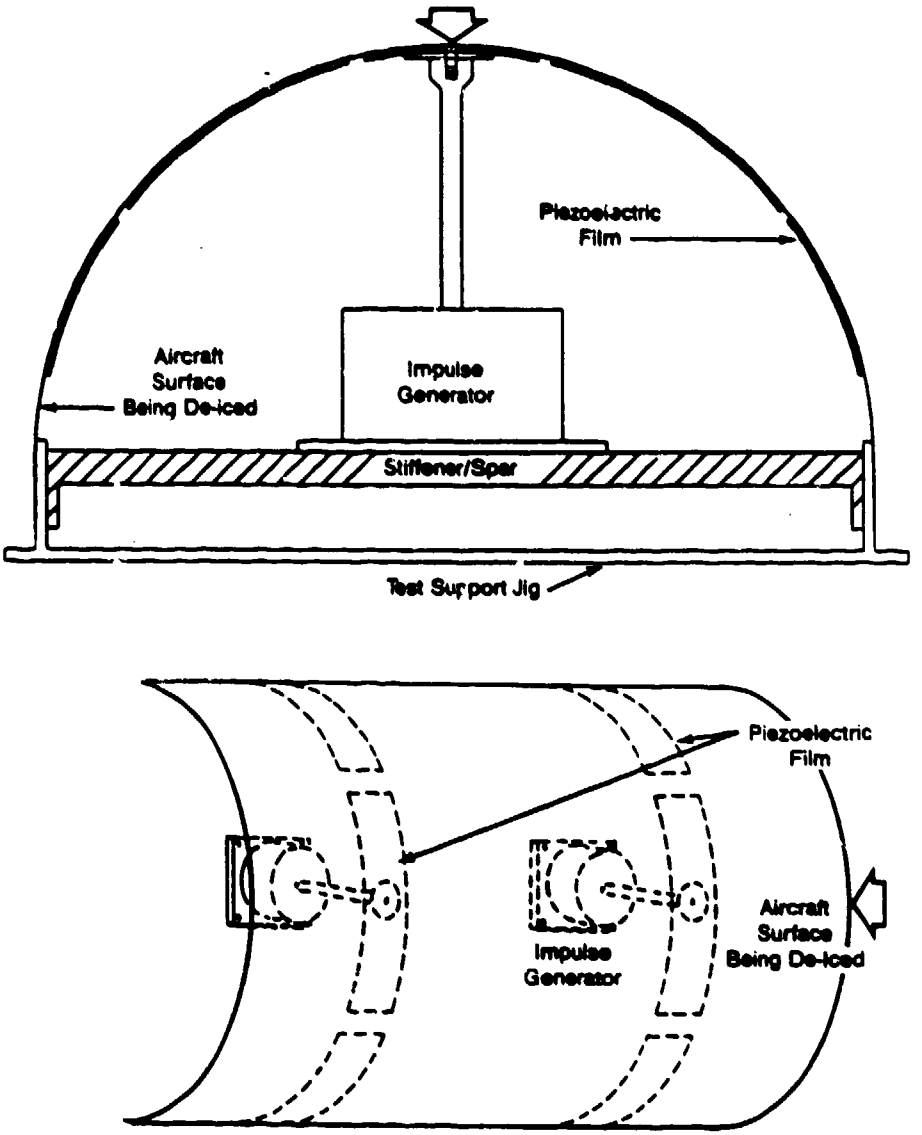

Figure 2-13. Piezoelectric Film Ice Detection/De-Icing System (General Arrangement)— Reference arrows indicate how these two schematic views relate to one another.

PULSE-ECHO. Ultrasonic pulse-echo ice detectors are being developed that operate by measuring the return rate of an acoustic signal reflected by a layer of accreted ice (Fig. 2-14). Ultrasonic acoustic waves from a transmitter are picked up by a receiver after being reflected from the ice layer on the aircraft's surface. During this transmission, the waves are reflected back and forth between the two surfaces of the ice layer. Multiple reflections (echoes) are required for the sound to bypass an acoustic block placed between the transmitter and receiver to prevent direct impingement of the signal from the transmitter onto the receiver. The time required for sound to travel from transmitter to receiver is directly related to the thickness of the ice layer. In addition to measuring the thickness of ice (in the range of .005 inch to .300 inch), this system is also capable of measuring the rate of ice accretion. Ultrasonic detectors may be contoured to fit flush with the leading edge surfaces, thus conforming to the aerodynamics of the aircraft.

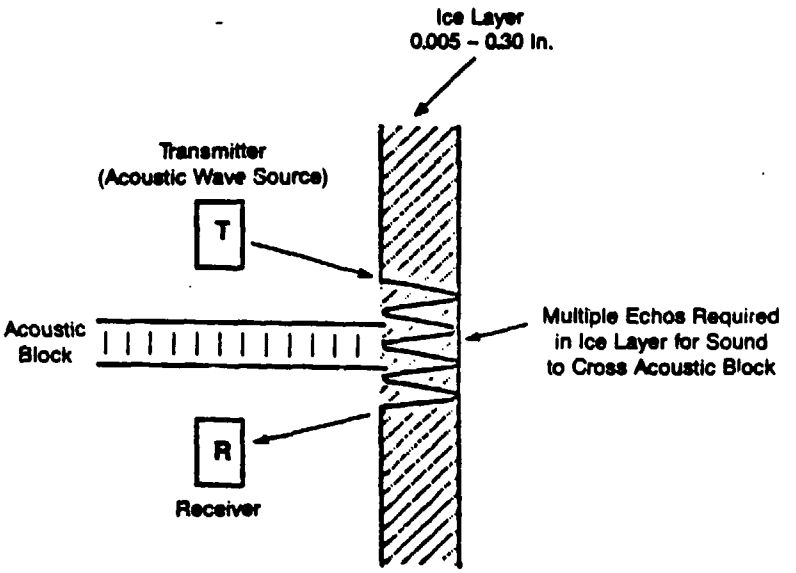

Figure 2-14. Ultrasonic Pulse-Echo Ice Detector Concept

OPTICAL. An optical ice detector suits the special requirements of helicopters. During hover or low-speed flight, ice detectors that require forward velocity may fail to indicate icing, although airflow into the engine (and icing) is high. One company has developed an ice detector and ice accretion rate sensor with a small suction device to induce airflow through a tube with a rod mounted across its diameter. The airflow through the tube is set to simulate the airflow into the engine inlet. A light shines across the front of the rod to a line of optical fibers. Ice that forms on the rod occludes the light, and the rate of shadowing on the optical fibers yields the icing rate. Periodic electric heating of the rod recycles the measuring system. When forward speed becomes excessive, however, the accuracy of the instrument deteriorates.

Several other types of ice detection systems were identified by the survey and the literature search; however, detailed information was restricted, primarily for proprietary reasons.

PHYSICAL PROPERTIES OF ICE.

Ice accretion on aircraft has been studied to determine the physical properties of the resulting ice layers. These properties have a direct bearing on the effectiveness of a de-icing system. Since it is not currently practical to measure ice accreted in flight, representative ice formation is studied under laboratory conditions. Experiments have been conducted to determine the mechanical properties of accreted ice and the stress required to fracture the ice (Ref. 3-1).

In one experiment, ice was generated by introducing 20-micron diameter water droplets into a high-speed cold airstream, which then impinged onto cooled metal plates. The ice density averaged 0.74 g/cm^3. Appearance of the ice was similar to rime ice (Ref. 3-2 and Appendix A). The thickness of the ice layers ranged from 0.75 to 1.5 mm.

Test samples consisted of 1.5 mm thick ice layers deposited onto aluminum plates. Both static four-point bend loading (Fig. 3-1) and constant strain loading of the ice were studied to determine the stress required to fracture the ice. The static loading tests measured Young's modulus of elasticity of the ice layers by recording the instantaneous deflection of the samples upon applying a load. Stress relaxation due to creep in the ice layers prevented fracture of the ice during static loading. The dynamic loading tests subjected the samples to a short initial acceleration period of increasing strain rate followed by a longer period of constant strain rate. The strain rates applied were in the range of 0.03 to 0.13 in/in-sec. The static Young's modulus measured for the ice samples was 2.85 GPa (413,000 psi).

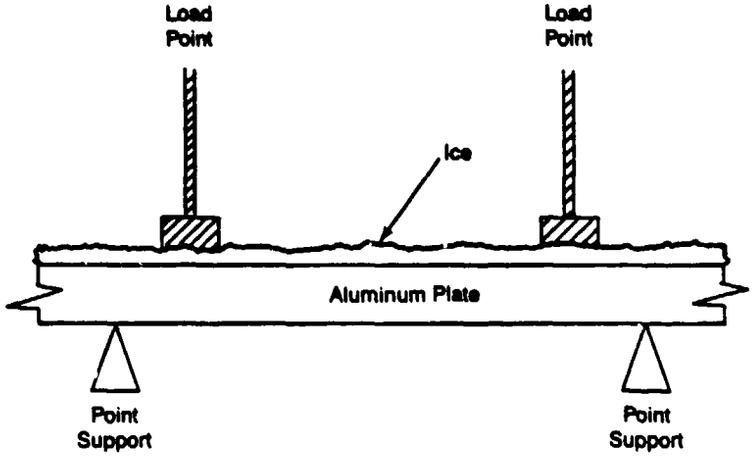

Figure 3-1. Four-Point Bend Loading

Results of the dynamic loading tests can be explained with a simple rheological model (Fig. 3-2), where E_1 is the instantaneous Young's modulus, E_2 is the transient creep elastic modulus and η_2 is the viscous creep factor (Ref. 3-3). The parallel loop represents transient creep with a decreasing strain rate. For polycrystalline ice, E_1 = 9.3 GPa (1,350,000 psi) (Ref. 3-4). Test results were E_2 = 3.8 GPa (551,000 psi), and η_2 = 27.9 MPa-sec (4,046 psi-sec). For this model, total strain, ϵ, can be expressed as:

$$\epsilon = \frac{\sigma}{E_1} + \frac{\sigma}{E_2} [1 - \exp (E_2 t/\eta_2)] \qquad \text{(Equation 1)}$$

where σ is stress and t is time.

A typical strain (ϵ) needed for fracturing ice, as determined by testing, is 1.5×10^{-4} in/in (Ref. 3-5).

Equation 1 may be a means of estimating the effectiveness of a mechanical de-icing system. For example, when de-icing is being modeled, the mechanical force-versus-time (the forcing function) transmitted to the ice layer can be specified. If the resultant strain exceeds the empirically determined value of ϵ stated above, it is probable that ice shatters and de-icing results.

The physical properties of ice are a function of formation conditions. In these studies, temperature was found to be the most influential variable. Temperature affects shape, quantity and strength of accreted ice and, hence, its aerodynamic properties and its propensity for shedding. Greatly reduced ambient temperatures may be associated with reduced liquid water content, which affects the type of ice formed. Other factors are altitude, aircraft velocity and water droplet size. In addition, net accretion is a function of time in icing conditions. Liquid water content and water droplet diameter do not have a significant effect on adhesive characteristics, although

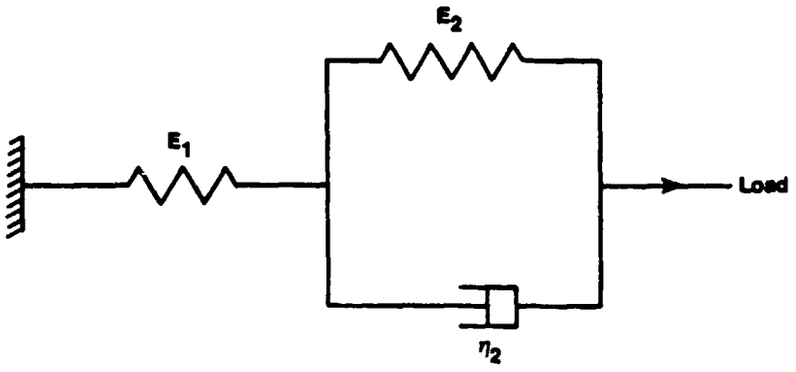

E_1 = Instantaneous Elastic Modulus
E_2 = Transient Creep Elastic Modulus
η_2 = Transient Creep with Decreasing Strain Rate

Figure 3-2. Rheological Model for Dynamic Loading Tests of Ice Strength

a slight reduction in ice strength was noted with increasing droplet diameter. Factors that may influence shedding characteristics are vibrations, changes in ambient conditions, or engine operating condition. This is particularly true for rotating surfaces where shedding may be deliberately induced.

COMPUTER ANALYSIS OF ICING AND DE-ICING.
The methodology proposed for evaluating the icing and de-icing phenomena of engine inlets involves the following steps: 1) determining the flow field in and around the inlet, 2) calculating the water droplet trajectories, 3) calculating the amount and shape of ice accretion on the inlet structure and 4) determining the trajectories of the shed ice fragments. Since accreted ice alters the inlet geometry, a more accurate solution requires repeating steps one through three with the new geometry. The engine manufacturer can use the information obtained this way to predict potential damage areas. Figure 3-3 is a flow chart of this process.

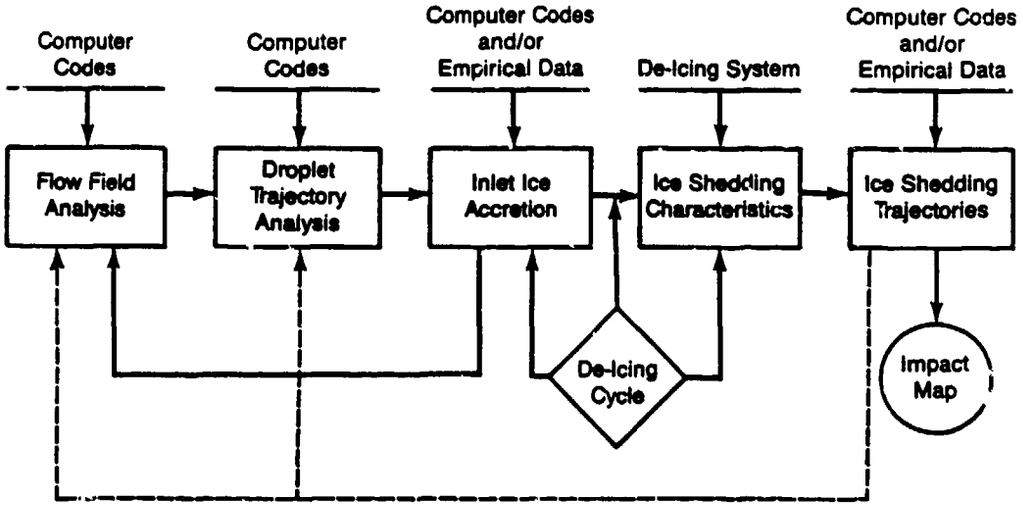

Figure 3-3. Icing/De-Icing Analysis Flow Chart

FLOW FIELD ANALYSIS. The first step in the icing analysis is to determine the flow field properties around the turbine engine inlet. This can be done using 3-D computer codes available in the literature (Refs. 3-6 to 3-13). Provided here is a list of extensively used 3-D codes for flow field analysis. Most of them are well-documented and available through government or commercial sources.

- Reyhner full-potential 3-D code--for transonic flow (Ref. 3-7)
- Hess/NASA-Lewis inlet code--for subsonic flow (Ref. 3-8)
- VSAERO code--for subsonic flow with compressibility correction (Ref. 3-9)
- PANAIR code--for subsonic flow with compressibility correction (Ref. 3-10)

Two criteria are suggested for choosing from the list above. First, the code should produce accurate velocities at arbitrary points in the regions of the body for airspeeds ranging from low subsonic to transonic. Second, the code should be validated by comparing predicted water droplet impact locations with experimental data.

These criteria are currently met only by the Reyhner code, which has been used extensively for inlet flow field analyses. This is the code used for the flow field input to the Kim trajectory and the water droplet impingement analysis (described in the following sections), which can be compared to new experimental water droplet impingement data now available (Ref. 3-14).

Unfortunately, the Reyhner code has been unavailable for general use; it has been Boeing proprietary information. The primary open literature source (Ref. 3-15) is essentially a user's manual and does not give program calculation details. By arrangement with NASA-Lewis, however, this program will become available in late 1988.

The Reyhner code is not a stand-alone code but requires a preliminary code to set up the inlet body geometry and relate it to the computation mesh (the mathematical representation of the geometry in computer language). The Boeing-proprietary set-up code, called MASTER (Modeling of Aerodynamic Surfaces by a Three-dimensional Explicit Representation), gives a precise surface definition with continuous first and second derivatives. It also defines all points of intersection of the mesh lines and the surface and provides interpolation equations. It is the intention of the NASA-Lewis Research Center to provide a similar set-up code when the Reyhner code is released.

Surface panel flow codes can be used for trajectory and impingement computations. However, a potential flow code that simulates realistic surface pressure distributions does not necessarily result in realistic droplet impingement distributions. A large number of small panels in the water impingement region will probably be required. If a curved surface is represented by a series of flat panels, the droplets may "see" the slope discontinuities and give distorted impingement distributions. The results can be expected to improve as the number of panels on the leading edge is increased or a special near-field computation method is used.

The VSAERO code is a candidate for further development in conjunction with a water droplet trajectory analysis (Fig. 3-4). It is generally available and widely used, and it produces good subsonic flow fields for nacelle inlets. This code uses surface singularities (sources and doublets) on quadrilateral

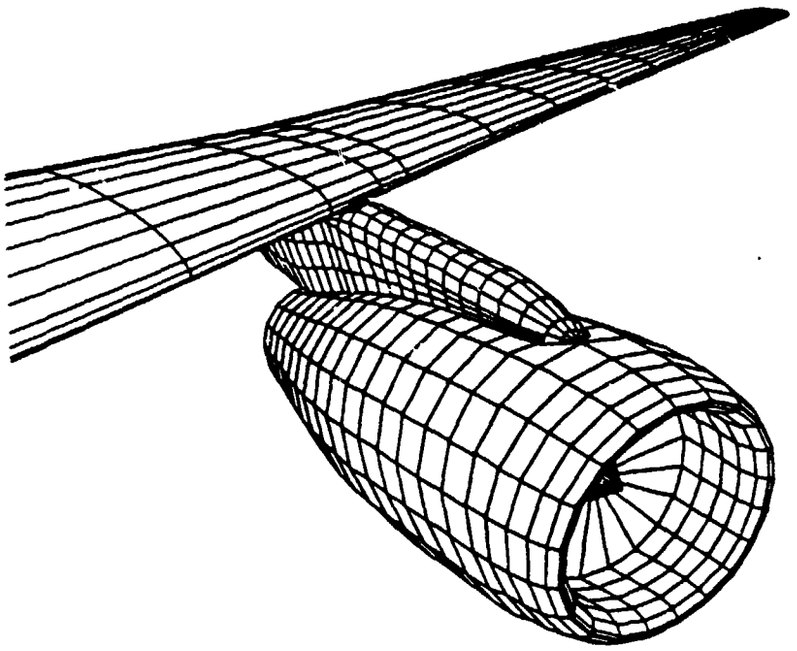

Figure 3-4. Surface Panel Modeling of a Wing, Pylon and Nacelle Using the VSAERO Computer Code

panels in a piece-wise constant manner. It is, however, limited to subsonic flows. Icing is infrequently encountered at higher subsonic or transonic flight speeds, since aircraft flying at these speeds are also flying at altitudes above icing conditions. However, icing analysis for this range is still necessary, because aircraft flying at low subsonic speeds may still experience sonic speeds of air inflow to an engine inlet, for example, during climb.

DROPLET TRAJECTORY AND IMPINGEMENT CODES. The next phase of the analysis is concerned with water droplet trajectory. This is a critical part in the analysis because the impingement information will be used to determine ice accretion rates. The input required for the droplet trajectory analysis is the flow field from a flow code and liquid water content (LWC) of the air in terms of droplet size and water mass per unit air volume.

The following list of droplet trajectory codes was selected using the same two criteria as those for the flow field analysis.

- Boeing 2-D droplet trajectory code
- 3-D droplet trajectory code—J.J. Kim (Ref. 3-16)
- 3-D droplet trajectory code—H.G. Norment (Ref. 3-17)

One of the strengths of the Boeing and Kim codes is that they are being compared to data acquired from new experimental impingement test carried out on axi-symmetric and 3-D inlets (Ref. 3-14).

ICE ACCRETION EVALUATION. Two methods are available for determining ice accretion on turbine engine inlets--computer code analysis and wind tunnel tests.

To use the computer code method, the first step is to determine the freezing positions of the impinging water, because it is at these positions that ice begins to accrete.

Because ice accretion alters the shape of the inlet lip, the flow field must be recalculated to account for the new shape of the inlet. Computer codes such as LEWICE (Ref. 3-18) can be used to predict ice accretion on 2-D airfoils in subsonic flows. Such 2-D codes have been substantiated with empirical data from wind tunnel tests. A study of the literature has revealed no existing 3-D ice accretion computer code.

Availability, time and cost may preclude the use of analytical tools for evaluation of ice accretion, especially for smaller aircraft companies. Alternative empirical methods of ice accretion evaluation are available, although not necessarily recommended. Researchers have empirically derived performance degradation equations based on many wind tunnel studies with 2-D airfoils (Ref. 3-19).

ICE FRAGMENT DRAG (C_dA). A suggested but as yet unproven method for adapting the droplet trajectory computer codes previously described to the determination of the trajectories of ice fragments shed from an inlet surface is described here. The adaptations are required because the sizes and shapes of shed ice are different from that of the spherical water droplets typically used in particle trajectory analysis.

The path of a shed ice fragment is due to the balance of gravitational and drag forces on the ice fragment. The drag force is calculated as C_dA (C_d = drag coefficient; A = surface area of fragment exposed to the airstream). Due to the irregular shape and size of shed ice fragments, specific drag coefficients have not yet been calculated. However, by taking into account ice fragment dimensions, C_d's may be estimated from data on C_d's of various body shapes (Ref. 3-20). For example, the C_d of a circular disk is 1.17 when aligned perpendicular to the flow direction, and the C_d for a hollow hemisphere can vary from 0.34 (concave side away from flow) to 1.42 (concave side facing flow). Because the ice fragments will be tumbling about their own axes, the fragments will expose a varying area, A, to the passing airstream. This area can be modeled by assuming that the tumbling ice presents a sinusoidally varying area to the airstream, i.e., $A = (2/\pi)$(geometric area) (Fig. 3-5). The C_dA term is now defined in a way that can be used in existing particle trajectory codes. Based on this, the engine components impacted by the shed ice can be determined, and, in turn, the potential for structural damage to these components can be assessed.

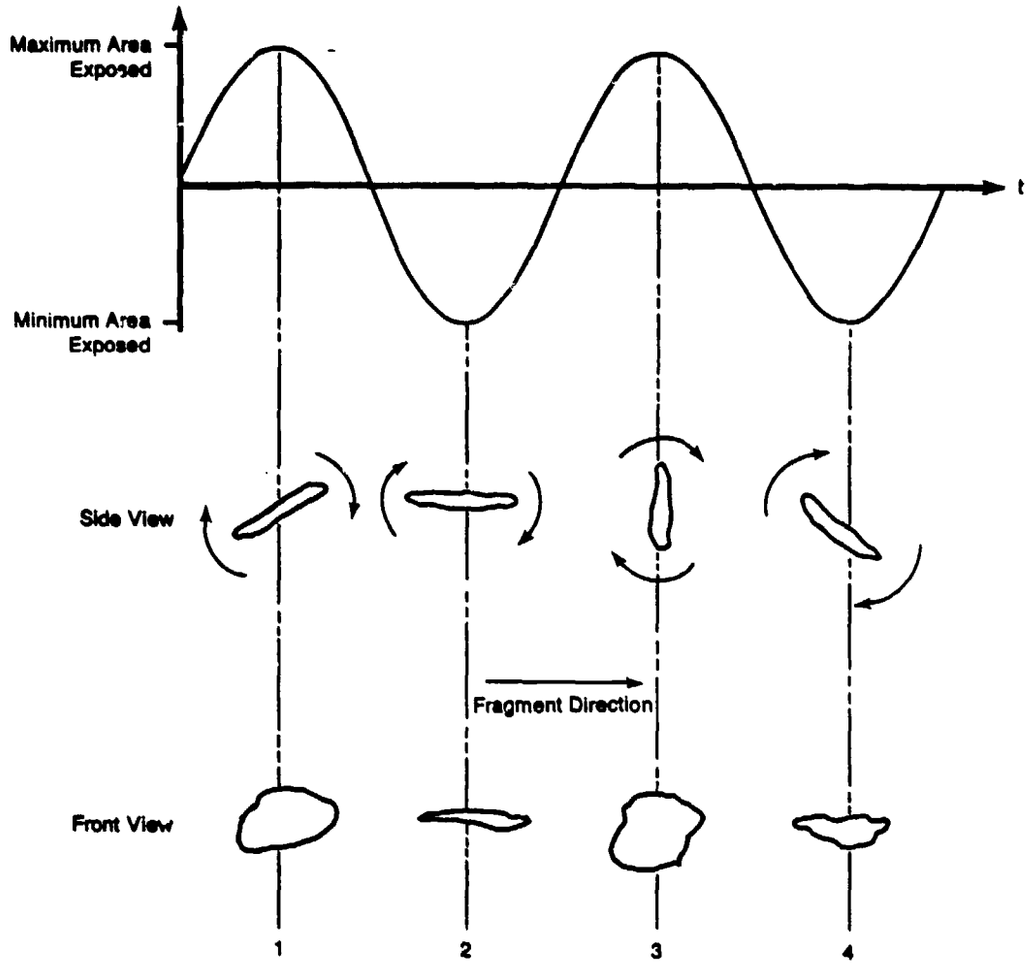

Figur 3-5. Cross-Sectional Area of Ice Fragment Presented to Airstream During Tumbling

WORST-CASE DE-ICING CONDITIONS.
De-icing systems must perform satisfactorily thoughout a range of icing conditions. This section discusses the worst-case icing conditions for the various de-icing systems.

ELECTROTHERMAL SYSTEMS. An electrothermal de-icing system is controlled by an electronic switching mechanism and is cycled according to a preprogrammed schedule. When designing such a system, the FAR Part 25 Appendix C icing envelope is used to determine and preset the power levels and timing cycles required for various icing conditions. Extremely cold conditions require high thermal power levels and maximum cycle on-times. Precision in the cycles becomes more critical as the ambient temperature increases, since the possibility of generating water runback and refreezing increases due to thermal lag and inherently higher LWCs. For this reason, ambient temperatures just below freezing generally represent the worst-case conditions for electrothermal de-icing systems.

CHEMICAL SYSTEMS. Published information on the use of chemical de-icers (freezing point depressants) in engine inlets is sparse due to the few, if any, uses of this type of system in commercial aircraft turbine engine inlets. Chemical systems will de-ice essentially in a manner similar to electrothermal de-icing systems, by breaking the adhesive bond between the ice and the aircraft surface; however, no water will be generated, thereby eliminating the runback/refreeze potential. The worst-case condition is generally where the ice/surface adhesive bond is greatest. High adhesive bonding is generally related to lower LWCs, lower temperatures (-14° to -22°F) and especially to low MVDs (below 15 microns). (MVD is droplet size measured as median volumetric diameter.)

MECHANICAL SYSTEMS. Mechanical de-icing systems, operating on the principle of shattering the ice accretions, typically operate best in the middle temperature range of the FAR Part 25 Appendix C icing envelope. The coldest icing conditions, while producing very hard and brittle ice, which is easier to shatter, usually result in very thin ice accretions due to correspondingly low LWCs. Also, the adhesive bond between the ice and the aircraft surface is high at the cold, low-LWC, low-MVD conditions. Even though the ice shatters in these conditions, the high adhesive bond reduces ice shedding. Since the ice accretions are thin and aerodynamically shaped, they should not have a significant effect on inlet aerodynamics. When the ice does shed, it is typically quite thin.

Since mechanical systems become effective at some minimum thickness, in the coldest, lightest icing conditions, several de-icing cycles may pass before the ice becomes thick enough for de-icing to occur. The use of variable timing for de-icing cycles would provide a solution for the coldest icing conditions.

The "warmest" icing conditions are also difficult for mechanical de-icers. In icing conditions just below freezing, ice accretions may have a slushy consistency. Since mechanical de-icers must shatter ice accretions to be effective, slushy ice represents the worst-case condition. With the high LWCs found in warm icing conditions, ice accretion rates are high and good de-icing performance is essential.

ENGINE MANUFACTURER'S ICING EXPERIENCE.
Measurements of shed ice fragments were conducted by a major engine manufacturer. The test inlet was a full-size (approximately 8-foot diameter) RB211 cowl and inner barrel assembly that could be rotated in the icing airstream to allow icing of large portions of the inlet.

During early EIDI de-icing trials, attempts were made to collect pieces of shed ice and measure their sizes. This was only partially successful, because it was never clear whether the collected pieces had actually been shed at the size they were found or whether they had broken up in flight or during impact with the catcher. It was concluded that the only definitive way to determine shed ice fragment size was to photograph the ice during and immediately after shedding.

A high-speed film video camera (400 frames per second) was mounted just in front of the inlet. It was focused on a region inside the inlet barrel extending from the inlet leading edge to about three feet rearwards. This section was painted black with a 2" x 2" white cross. The black paint was intended to increase the visibility of the ice fragments as they were being shed, and the white cross was to be used as a reference for estimating the fragment sizes.

It was found that the trajectories of the ice fragments brought the fragments toward the camera as well as back through the inlet, making them appear larger in relation to the white cross than they actually were. Because the actual trajectory was not known, no correction could be made for this effect. Fragment size estimates could only be made during a short period immediately after the ice had been shed and before its trajectory brought it away from the inner barrel.

This experience has led to a possible technique for improving the method for determining the fragment size of shed ice. Instead of one camera, two cameras should be used, pointed in orthogonal directions. (In the case just described, for example, a second camera mounted above the first camera and pointed downward would be used.) The entire background (e.g., inlet inner barrel, wing surface, etc.) should be painted black to make ice fragments more visible, and a continuous grid should be used instead of the white cross to make size measurements easier. Camera speed (typically 300 - 1,000 frames per second) should be chosen according to the speed of the airstream around the inlet.

Use of the above technique to measure shed ice fragment sizes and possibly trajectories may provide empirical data necessary to substantiate future shed ice fragment trajectory computer codes.

SAFETY REQUIREMENTS SUBSTANTIATION

ALLOWABLE ICE ACCRETION.
The primary hazard associated with engine inlet icing is the potential for damage caused by shed ice that is ingested by the engine. Secondary effects of ice buildup are the possibilities of inlet airflow distortion and blockage, which could affect engine performance.

Analytical methods described in previous sections address the ice accretion rate, de-icing effectiveness and the size of ice fragments released. These methods may be used to determine whether a de-icing system should be considered for an engine inlet. Currently it may be possible to estimate ice accretion rates using the codes described in the Computer Analysis of Icing and De-Icing section. These codes are based on empirical studies in simulated icing conditions. Information regarding the shapes and aspect ratios for ice fragments shed from the inlet during system operation is best acquired from the same empirical studies. This can give rough estimates of the ice fragment sizes that might be ingested by the engine.

ENGINE PERFORMANCE WITH INLET ICE. Ice accretion rate is a function of inlet shape, meteorological conditions, and aircraft/engine operating conditions. The maximum ice thickness that accretes on an engine inlet will be determined by the particular de-icing system used. A properly designed system will keep ice layers thin and therefore aerodynamically shaped, so that ice on the inlet presents a minimal concern for engine operation.

Some turboprops are currently certified for flights into icing conditions with engine inlets that are de-iced by pneumatic boots. Although these turboprop inlets are small, their engine performance is not significantly compromised by an ice thickness of 1/4 inch—the maximum ice thickness at which these de-icing systems are optimally effective (see Pneumatic Boot section.) Turbofan engines have equal or greater sized inlet flow areas than the turboprops. For this reason, an ice accretion of 1/4 inch should not adversely affect their operation if de-icing were to be used on the engine inlets of these aircraft. Furthermore, it is expected that the new de-icing systems will keep ice maximum thicknesses to less than 1/4 inch (see De-Icing section), and ice accretion will be even less of a concern for inlets using these new systems.

ALLOWABLE ICE INGESTION.
The effects of ice ingestion on the engine are taken into consideration during standard design analyses carried out by aircraft turbine engine manufacturers. All aircraft turbine engines have an acceptable level of ice ingestion. Allowable ice ingestion can be defined in two ways: 1) maximum ice fragment size or 2) maximum ice fragment quantity during a de-icing cycle. For any turbine engine, one definition will result in a stricter limitation on ice ingestion than the other; however, for many engines, it may be advisable to define both values.

The limit on ice fragment size is usually set to be that which prevents any impact damage to engine components. The limit on total quantity of ice ingested during one de-icing cycle is defined as the limit above which the ice will cause an intolerable shift in engine operation, such as that which might cause engine surge or stall.

Operation of a de-icing system could presumably result in acute damage to an engine due to an infrequent shedding of large ice fragments into the engine blades or other components. For both rime and glaze ice types, such an encounter is expected to result in a definable ballistic type of soft-body (bird-type) threat to the engine structure. Under such conditions, it should be possible to determine whether or not damage has occurred and, if so, whether engine operation has been impaired.

Many turbine engine manufacturers use analytical methods to predict engine ice ingestion capability; however, these methods are proprietary information. Computer codes developed by engine manufacturers for structural impact analysis are empirically substantiated by ice ingestion tests conducted to fulfill FAR Part 33 engine ice ingestion certification tests as well as other ice impact tests.

Whether or not a particle separator is used in an inlet will directly influence the process of matching an engine with a particular inlet de-icing system. Although a particle separator will not affect the ice ingestion tolerance of a turbine engine, it will allow shedding of larger fragments and quantities of ice from the inlet, because, depending on the performance of the separator, most, if not all, shed ice will bypass the engine.

Probably a more realistic concern than inadvertent release of large quantities of accreted inlet ice is the regular release of relatively small fragments and quantities of ice. The turbine engine manufacturers must determine the level of ice ingestion below which engine component damage will not occur and engine power output will not be affected. Simultaneously, de-icing systems must be evaluated to determine if they will shed ice of suitable size and quantity such that engine ingestion limits are met. The possibility of engine component erosion resulting from repeated ice impacts may prove to be more of a cost-maintenance concern rather than a flight safety issue.

Cumulative engine damage due to these less severe but repeated ice impacts resulting from de-icing in normal flight envelopes should be addressed in testing. Such tests should define shed ice fragment size (at least in thickness) that occurs under such flight conditions and an assessment of the total number of these fragments that will be encountered in a given flight. The engine manufacturer should evaluate the engine blading and structure under such an environment, as well as the continued operation of the engine following any such damage. This, in effect, would require the manufacturer to define acceptable damage limits for the engine and to provide controls that would maintain engine operation following damage within these limits.

ICE IMPACT EFFECTS ON ENGINE COMPONENTS.

Ice released from the inlet as a result of de-icing generally follows a flow streamline through the inlet and impacts the fan at approximately the same

radius relative to the engine center line at which it was released (Fig. 4-1). Considered here are the effects of ice impacts on various components of the engine--both those that occur directly and those that result from ice shattered by the fan.

ACOUSTIC LINERS. For turbine-engined aircraft to comply with applicable noise regulations, much of the inside of their engine inlets and bypass ducts is covered with acoustic liners (Fig. 4-1).

Areas where acoustic liners might be located are:

Area A—Between inlet leading edge and fan face
Area B--In and just to the rear of the fan rotor path
Area C—Along the bypass duct rearward of the fan

AREA "A" LINERS. The engine inlet diameter is generally smaller than the fan face diameter. Thus, ice released from the inlet leading edge usually does not impact the acoustic linings in the area forward of the fan. An exhaustive search of reported service incidents covering over 24 million flying hours on all RB211 engines has revealed no incidents of damage to the acoustic liners of area "A" that could be attributed to inadvertent shedding of ice.

AREA "B" LINERS. Ice can build up on the fan blades and create an out-of-balance condition. The accepted procedure in this situation is to dislodge the ice by increasing the engine speed for a short period. The dislodged ice may slide towards the tips of the fan blades following a path that is determined by the blade shape and fan speed. The liners in th! area should be designed to withstand this type of repeated ice impact.

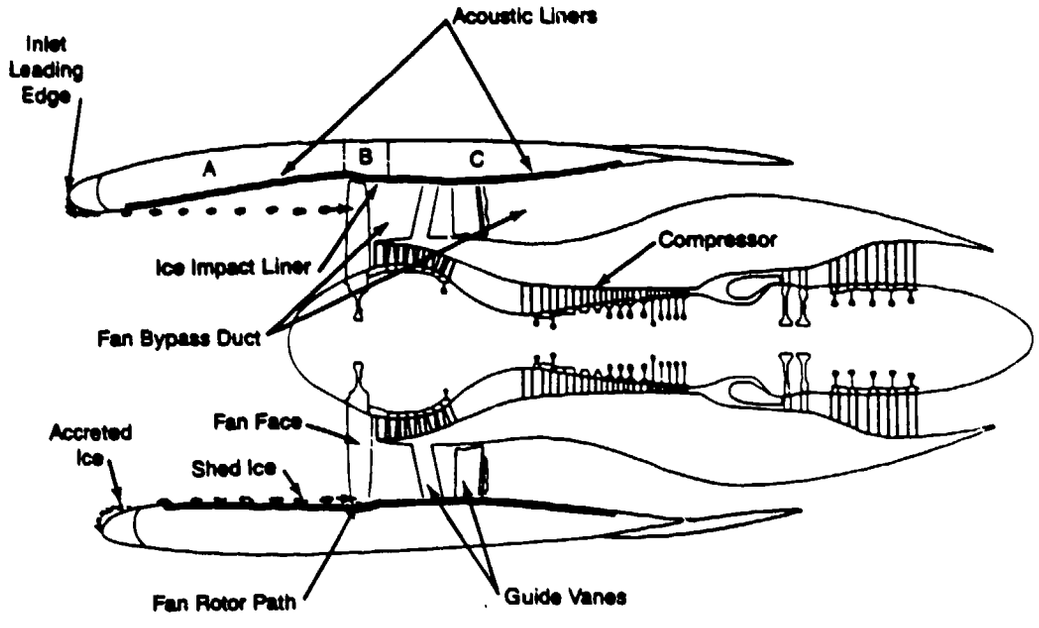

Figure 4-1. Initial Path of Ice Shed from Engine Inlet Leading Edge—Acoustic liners of the engine nacelle in areas A and C are relatively free from ice impact, but the liner area B is subjected to ice impact as a result of ice dislodged from the fan.

Ice released from the engine inlet tends to follow a streamline through the engine and strike the fan near the outer edges of the blades. This impact with the fan shatters the ice and imparts high values of both tangential and axial velocity to it. Due to the axial velocity, it is possible for this ice to miss the ice impact liner of area "B" and hit the acoustic lining aft of the impact lining. However, because this ice passes through the fan close to the blade tips, it would hit the liners with only glancing blows. Within the ice impact region (area "B"), these glancing blows have much less force than those imparted by ice shed from the fan blades, for which this area liner is designed. This is substantiated by RB211 service records. In over 24 million flying hours, only three engine inlets have experienced ice impact damage to the liners of the fan rotor path. Damage to two of the inlets occurred on the same aircraft during the same experimental flight. The other incident occurred on an aircraft where the center engine was thought to have ingested ice dislodged from the fuselage. Both aircraft were undergoing specific ice testing trials at the time, prior to certification.

AREA "C" LINERS. After passing through the fan blades, ice follows a path parallel to the liner surface. It therefore has zero velocity (zero impact momentum) in a direction perpendicular to the liner's surface. With no velocity normal to the surface, the ice passing through the outlet guide vanes (OGVs) and down the bypass duct does not cause any damage to the liners in these areas. The search of reported service incidents for all RB211 engine types has revealed no damage in area "C" that could be attributed either to ice shed from the fan blades or ice shed from the inlet.

ENGINE COMPRESSORS. On most modern large turbofan engines, the diameter of the fan inlet is significantly greater than the diameter of the core compressor inlet. Since ice released from the fan inlet would be expected to hit the fan blades at approximately the inlet radius, it would not likely be ingested into the compressor core. Thus, damage should not occur as a result of ice being shed from the fan inlet and directly impacting the compressor blades. There is the possibility, however, that damage to the compressor could occur indirectly by ice damaging the fan blades and causing engine surge as a result.

A review of all RB211 service engine incidents since 1972, revealed that a recorded total of 47 aircraft have experienced ice/snow ingestion that has affected 56 engines. The majority of these incidents resulted in little or no damage. However 14 engines sustained fan blade leading edge damage, and secondary damage to the intermediate- and high-pressure compressors occurred as a result of engine surge. All incidents involved the center engine of a tri-engine transport aircraft. This finding highlights the need for de-icing and snow removal from the fuselage and center engine inlet S-duct, a requirement that has not always been recognised during the early operation of this aircraft. In no case, however, can core damage be directly attributed to ice released from the engine inlet as a consequence of de-icing.

INLET GUIDE VANES. No information was obtained from engine manufacturers regarding tolerance to ice damage of inlet guide vanes, which are found in front of the fan blades on some, generally older, engines.

Many engines are equipped with outlet guide vanes (OGVs), which function to remove the rotational components of the airflow leaving the fan blades. Ice that passes through the fan has been shattered and has had high values of tangential and axial velocity imparted to it. This results in ice passing through the OGVs at low-incidence angles without causing damage. A search through all RB211 service incidents in which ice was thought to be involved confirmed that no damage occurred to OGVs. Engine service records from other engine manufacturers were not available for confirmation of these conclusions.

FAN BLADES. Fan blade damage could occur if sufficiently large pieces of ice were released from the engine inlet. Impact studies performed by engine manufacturers using both ice and birds (real and simulated) have demonstrated a high correlation between permanent deformation of fan blade leading edge and the kinetic energy of the bird/ice normal to the surface of the blade's leading edge. A kinetic energy threshold (V_{crit}) can be determined, above which damage occurs to the blade, and below which no damage occurs (Fig. 4-2). By comparing a family of curves obtained from impacts at different positions along the length of the fan blade, it is found that as impacts occur closer to the fan tip, the damage-versus-kinetic-energy curve becomes steeper. Particularly at the blade tip, once the kinetic energy threshold has been exceeded, a small increase in kinetic energy will result in a relatively large increase in permanent blade deformation. Ice released from the engine inlet will most likely impact near the tips of the fan blades in this region of high sensitivity to kinetic energy.

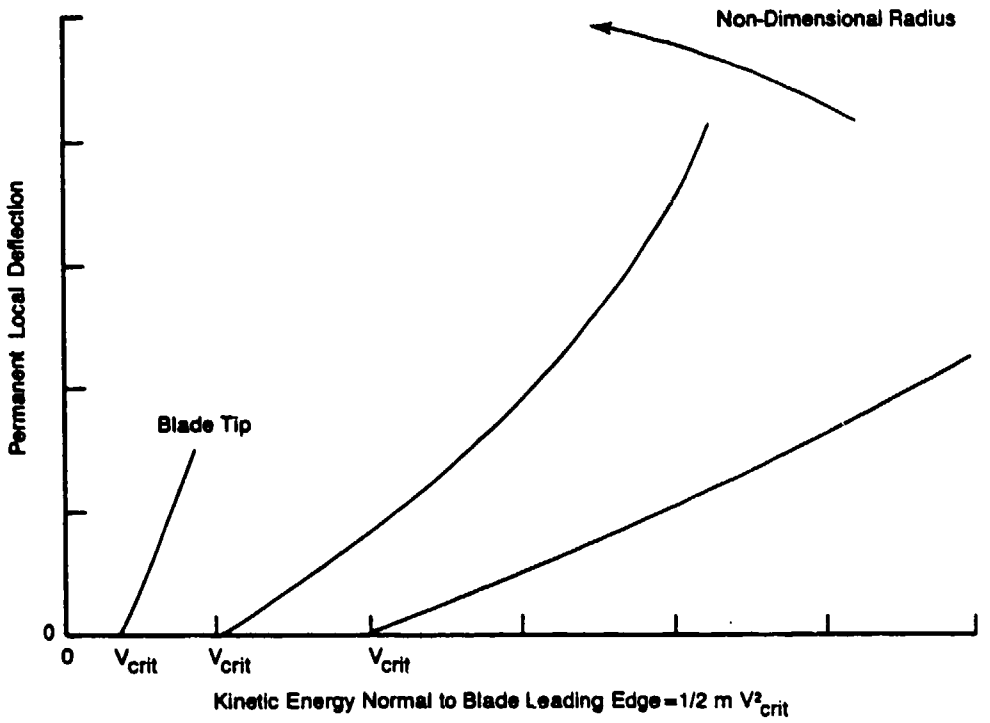

Figure 4-2. Relationship Between Kinetic Energy Normal to Fan Blade Leading Edge and Fan Blade Damage

METHODOLOGY FOR DETERMINING FAN BLADE DAMAGE. Ice is very likely to impact the fan blades near their tips, where they are most vulnerable to damage. Therefore, rather than attempting to assess graded levels of "safe" damage, it is considered safest to determine the maximum ice fragment size that causes no fan blade damage. One possible method for calculating this is presented here. The method is deliberately generalized so as to be applicable to different fan blade designs, flight conditions and engines operating in different aircraft.

The method determines whether the calculated velocity of an ice fragment (V_n) as it hits the fan blade is above or below the threshold velocity (V_{crit}) that causes fan blade damage for a given ice fragment of given mass. It is based on the threshold levels of kinetic energy normal to the blade, $1/2\ mV^2_{crit}$, determined from impact studies for both wide-chord and narrow-chord, shrouded blade types. The methodology is as follows:

	Procedure	Considerations
Step 1	Select ice fragment size and calculate	• Based on wind tunnel studies
Step 2	Calculate velocity of ice fragment entering fan blade row.	• Engine flight condition • Inlet length
Step 3	Calculate component of relative velocity normal to blade leading edge (V_n).	• Blade geometry • Assumed impact radius
Step 4	Compare V_n with V_{crit}. If $V_n > V_{crit}$, go back to Step 1 with smaller ice fragment. If $V_n < V_{crit}$, then no damage.	

STEP 1. The initial step is to select the size of ice fragment that might be released from the inlet and calculate its mass (m). (The ice is assumed to have a specific gravity of 0.9.)

STEP 2. Once the ice fragment has been released from the inlet, it will be accelerated by the airstream toward the fan blades. The accelerating force on the fragment, F, at any instant will be:

$$F = 1/2\ C_d A\ \rho_{air}\ (V_{air} - V_{ice})^2 = m\ \delta V/\delta t$$

where:

C_d = drag coefficient of shed ice fragments (C_d is dependent on fragment shape. Drag coefficients for different fragment shapes can be found in Reference 4-1.) In the following example, C_d = 1.0.

A = cross-sectional area presented by ice to the airstream; this is taken as an average area, assuming the ice fragment tumbles thereby presenting a sinusoidally varying area to the airstream, i.e., $A = (2/\pi)$(geometric area). (See Fig. 3-5).

ρ_{air} = density of the air; this parameter varies with flight conditions such as altitude.

V_{air} = airstream velocity; the velocity used is that occuring at the fan face.

Note: For these calculations, it is assumed that the ice fragment tumbles in such a way that, on impact with the fan blade, it is oriented so that the whole mass of the ice fragment impacts one fan blade. This is a worst-case assumption on average, since it is most likely that the impact of the fragment will be divided between two blades as shown in Figure 4-3.

V_{ice} = ice velocity

m = ice mass = $(\rho_{ice})(Vo_{ice})$, where ρ = density; Vo = volume

$\delta V/\delta t$ = velocity increase per unit time (δt)

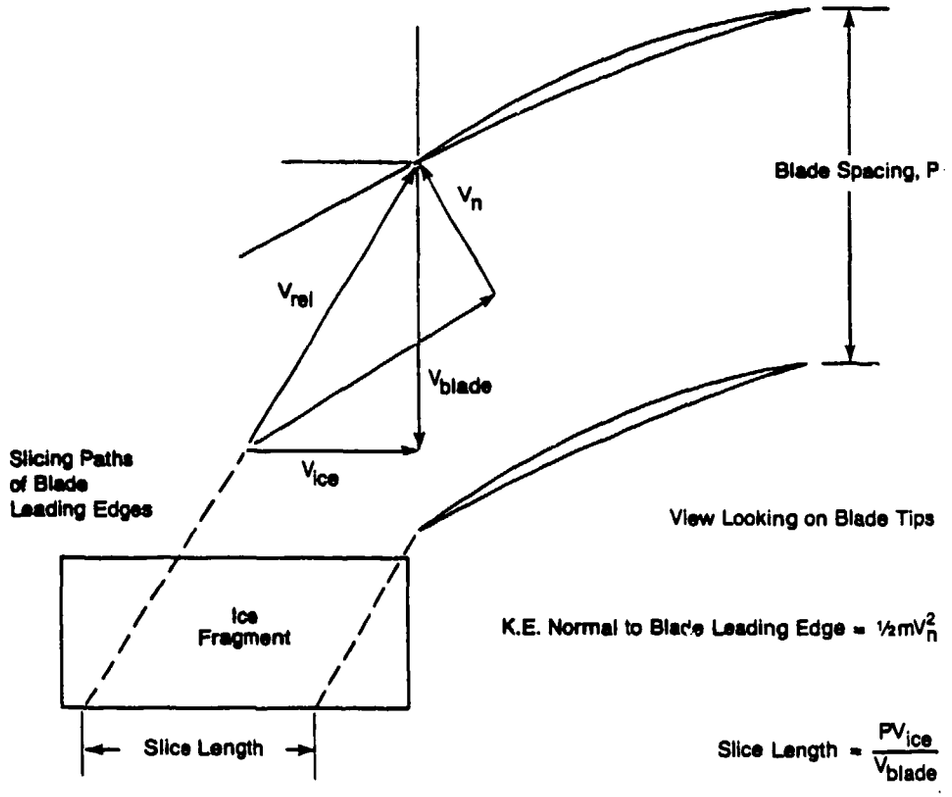

Figure 4-3. Velocity Triangles of Ice Impact at Fan Blade Leading Edge

A simple computer program can be written, with small time increments, δt, that enables the ice velocity to be derived for any inlet length. The typical relationship between ice velocity and inlet length is shown in Figure 4-4.

STEP 3. It is assumed that the ice will strike the fan blade row at the same radius (R) as that of the inlet from which it was released. From the geometry of the blade, the blade velocity (V_{blade}) and the ice velocity (V_{ice}), a velocity triangle can be constructed to determine, V_{rel}, the velocity of the ice relative to the moving blade. Then, V_n, the component of the relative velocity of ice normal to the blade leading edge can be determined from the velocity triangle (Fig. 4-3).

STEP 4. The value of V_n obtained from Step 3 can then be compared with the value of V_{crit} (the maximum value of V_n for which there is no blade damage) obtained from Figure 4-5 or Figure 4-6, depending on whether the blade is of the wide-chord or the narrow-chord type. The mass of ice used is that obtained from Step 1 and the non-dimensional radius, R, for the strike radius is the same as that used in Step 3.

If V_n is greater than V_{crit}, the ice fragment size determined in Step 2 is likely to cause damage to the blade, and this process of comparing V_n with V_{crit} is repeated for a smaller ice fragment.

If V_n is smaller than V_{crit}, then no fan blade damage would be expected from the size of ice fragment selected.

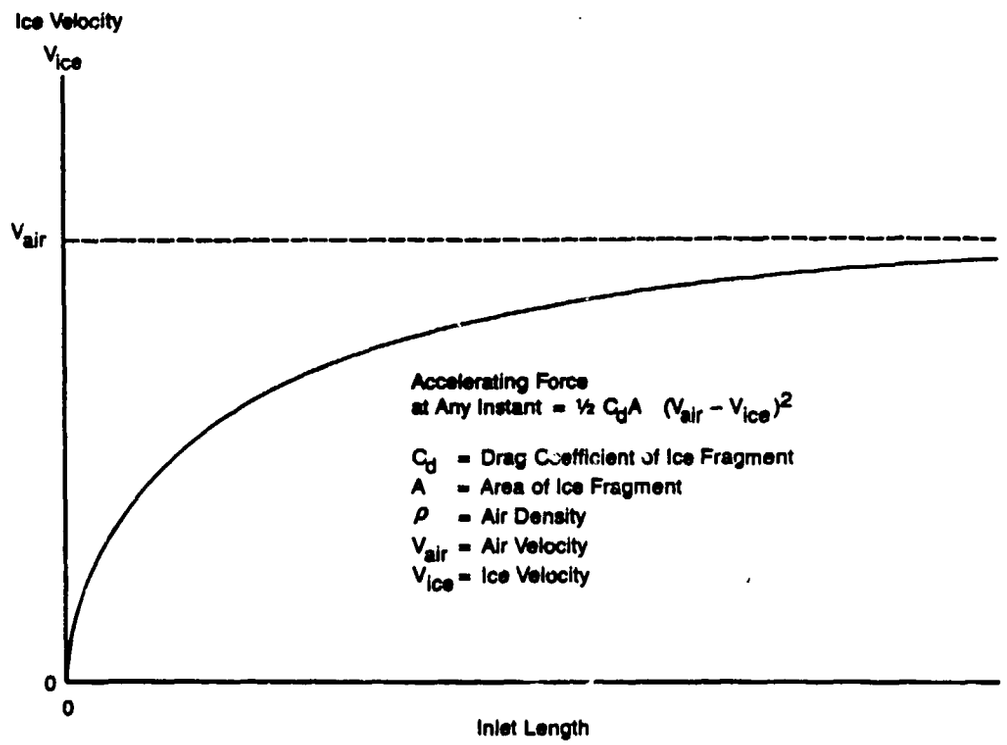

Figure 4-4. Typical Profile of Ice Velocity Increase with Engine Inlet Length

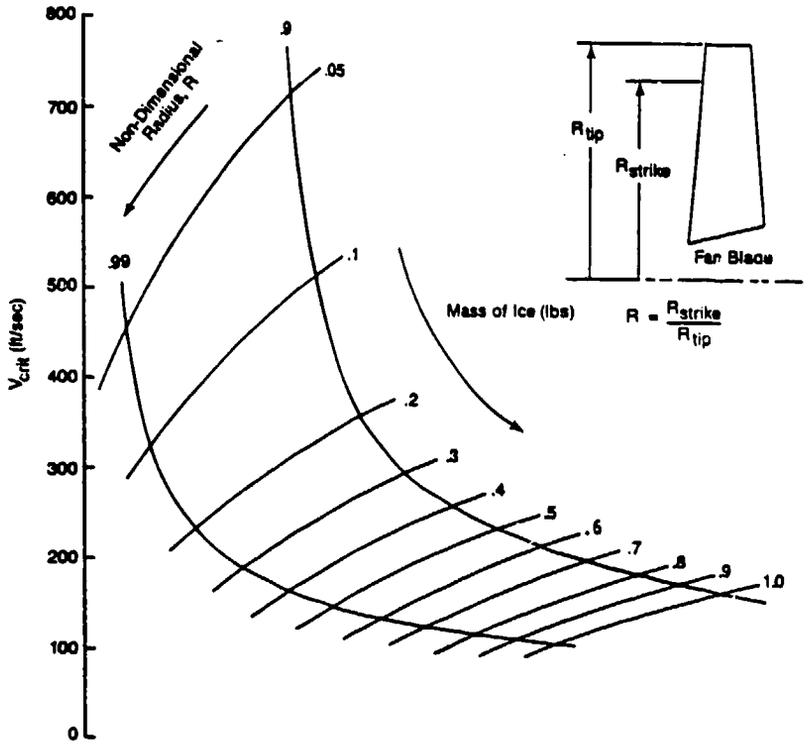

Figure 4-5. Variation of V_{crit} with Ice Mass and Non-Dimensional Fan Blade Radius (Wide-Chord Fan Blade)—V_{crit} = Threshold Velocity of Ice Fragment Above Which Damage Occurs to Blade

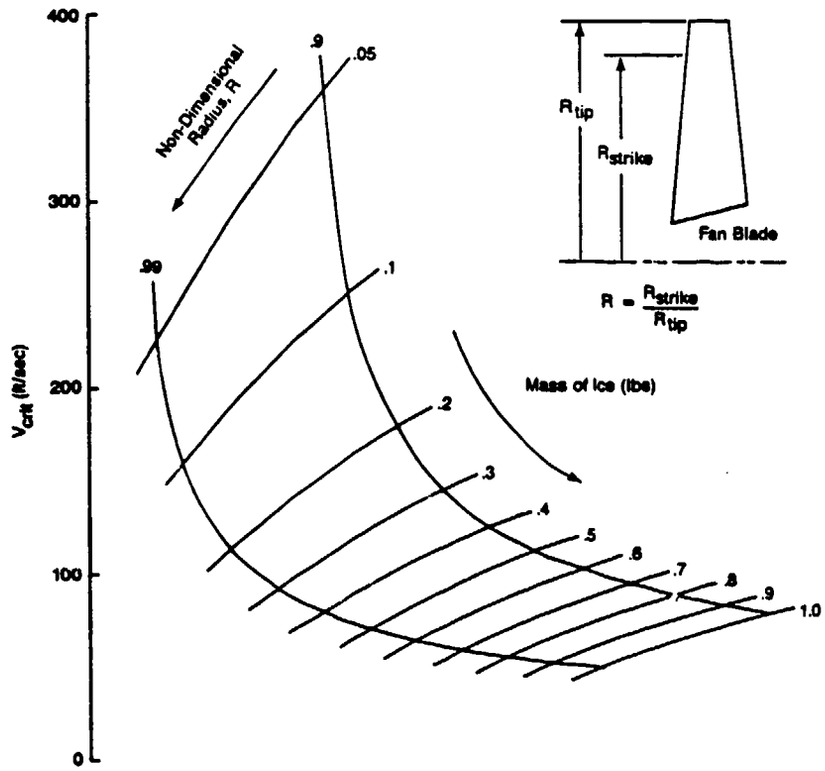

Figure 4-6. Variation of V_{crit} with Ice Mass and Non-Dimensional Fan Blade Radius (Narrow-Chord Fan Blade)—V_{crit} = Threshold Velocity of Ice Fragment Above Which Damage Occurs to Blade

An example using this method is given below:

Basic conditions:	engine	RB211-535C
	fan speed	1750 rpm
	inlet airspeed V_{air}	250 ft/sec
	flight condition	descent at 10,000 ft
	density of air at 10,000 ft	0.0563 lb/ft^3
Assume:	ice fragment size	12"x14"x0.125"
Calculate:	ice fragment mass	0.194 lb
	average area presented to airstream	0.212 ft^2
	velocity of ice at fan face, V_{ice}	86.2 ft/sec
Given:	blade velocity at 90% blade radius	511 ft/sec
Calculate:	normal velocity onto blade leading edge, V_n	161 ft/sec
From Fig. 4-6:	value of V_{crit} for R = 0.9, m = 0.194 lb	186 ft/sec

Hence, since $V_n < V_{crit}$, no damage would be expected.

The results of the impact studies (Figs. 4-5 and 4-6) demonstrated that above the threshold level (V_{crit}), damage increases very rapidly even for a relatively small increase in ice fragment mass or fan blade radius, particularly at the tip of the blade. For this reason, trying to set some acceptable level of fan blade damage becomes impractical.

ICE FRAGMENT CURVATURE. As previously stated, a conservative assumption has been made with regard to the orientation of the ice fragment—that the whole fragment hits one fan blade. It is also assumed that the fragment is rectangular and flat, which, for purposes of calculating the impact force imparted to the blade, is adequate. However, ice shed from the inlet is actually curved, the curvature resulting from the shape of the inlet on which it was formed. Because of this difference in shape, the rectangular mass of ice that is assumed to impact the blade leading edge has a greater velocity normal to the blade, and thus a greater force, than the curved ice that actually impacts the blade. Figure 4-7 compares the flat and curved ice fragments in their worst-case attitudes relative to the blade.

CORRELATION OF V_{CRIT} TO ICE FRAGMENT MASS AND POINT OF IMPACT ON BLADE. As expected, the threshold velocity at which damage occurs to a fan blade (V_{crit}) is correlated with the mass of a bird or ice fragment

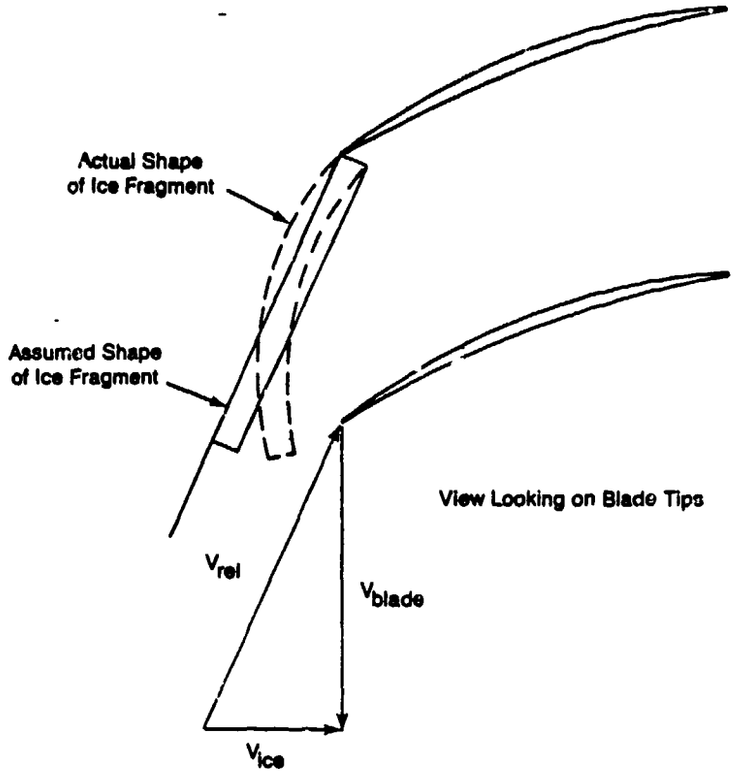

Figure 4-7. Curvature of Ice Fragment Impacting Fan Blade

impacting the blade (Figs. 4-5 and 4-6). In addition, as the site of impact for a given mass of ice moves from base to tip of the blade, damage occurs at lower and lower velocities (V_{crit} decreases). In Figure 4-5, the curve for R = 0.9, is based on data from tests in which rotating blades were hit by birds, and the curve for R = 0.99 is based on data from tests in which cylinders of ice impacted stationary blades statically clamped at their bases. The use of bird (i.e., soft-body) data to predict damage resulting from ice fragment impact is justified on the basis that the internal stresses generated in the ice cylinder substantially exceed ice tensile strength. Therefore, both can be treated as fluid jet impacts. The similar densities of ice and bird result in similar impact pressures on the fan blade (Refs. 4-2 and 4-3).

GENERALIZATION OF METHODOLOGY TO OTHER APPLICATIONS. It is not feasible in this document to cover all combinations of engines, fan blade designs, flight conditions and ice fragment sizes. This method will require adaptation for use in applications other than the engines studied. For example, the criterion of "no damage" is based on large turbofan engines (both wide-chord and shrouded, narrow-chord types) for which this methodology has been substantiated by reviewing service records. Other turbine engines may be more or less prone to fan blade damage from bird and ice ingestion. Therefore, it would be necessary to derive V_{crit} for each particular fan blade design.

GENERAL STRUCTURAL ANALYSIS OF IMPACT DYNAMICS.

It is expected that ingested ice fragments will impinge on the forward parts of the engine structures, such as the inlet guide vanes or fan blades. Recent research on foreign object damage to fan blades has resulted in the development of a variety of analytical techniques that describe and predict the impact process and structural response of the blades. The purpose of this section is to outline these analytical procedures.

APPROACH 1. First, ice fragment trajectories are determined (see the Computer Analysis of Icing and De-Icing section). Based on this information, sites of impact on the engine and impact velocities can be obtained.

Next, a model for the dynamics of the ice impact process (Ref. 4-4) is developed, based on non-viscous fluid mechanics theory. This type of analysis is independent of the compressive strengths of the impacting ice and uses potential flow theory represented by complex mathematical analysis to model the ice impact. This, in turn, predicts the pressure distribution on the impacted surface.

Figure 4-8 pictorially describes the process, wherein a bird (or other soft-bodied object such as ice) impacts a target at a velocity, V, causing a shock velocity, V_s, to propagate in an opposite direction and energy to be released tangentially to the surface. This energy release sets the pressure distribution on the surface. Once the pressure distribution is known, this data can be transferred to structural dynamics codes (e.g., NASTRAN) to determine the blade response characteristics under ice impact.

APPROACH 2. Another available approach makes use of the DYNA3D computer code (Ref. 4-5), an explicit three-dimensional, finite element code for analyzing large deformation responses of inelastic solids and structures. This code can model 26 materials using 11 equations of state to analyze a wide range of material behavior. The code contains an algorithm that simulates sliding interfaces and ballistic impact.

One of the code's useful features is the capability to model local failure of the selected model mesh. This modeling of the breaking apart of the structure is realized by using element corners that disconnect when a defined plastic strain is achieved. Hydrodynamic modeling is also available, which means that the code could be used to completely characterize the ice impact process.

SAFETY ISSUES OF DE-ICING SYSTEMS.

Safety becomes a concern if the use of a de-icing system results in damage to an engine's fan blades or other components. Currently, the designer of the de-icing system works with the engine manufacturer to determine the compatibility of a de-icing system with an engine. The engine manufacturer specifies the fragment size and amount of ice that can be ingested by the engine without damage. The de-icing system manufacturer then designs his system to operate within these specifications.

Service experience has indicated that blade damage poses a threat to safety only when it exceeds that which occurs as a result of impacts by multiple

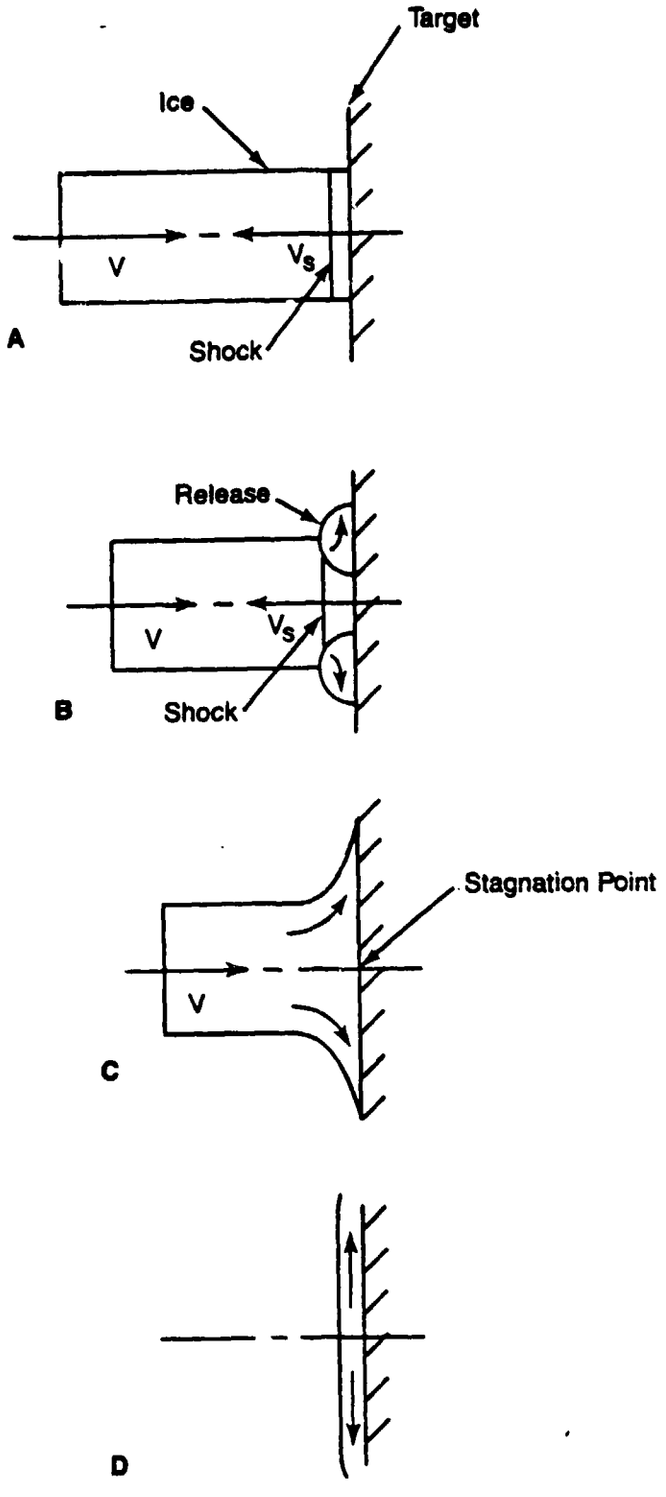

Figure 4-8. Phases of Ice Impact—(A) Initial Impact, (B) Impact Decay, (C) Steady Flow and (D) Termination (Ref. 4-4)

1-1/2-pound birds as demonstrated by medium-sized bird ingestion tests currently conducted under FAR 33.77. It is the opinion of one engine manufacturer that replacing an ice-damaged blade will be a maintenance concern to the aircraft user rather than a serious safety consideration. A de-icing system that releases ice fragments which cause small dents to the blade edges could, after several icing encounters, cause cumulative denting that finally exceeds acceptable limits with respect to the engine manufacturers' maintenance specifications. This, then, becomes an economic concern for the aircraft user, who must decide whether to replace or to repair the blades. According to one engine manufacturer, this cumulative denting only becomes a safety issue if it exceeds the medium-sized bird strike damage, which may be a factor of 100 or more greater than the ice-caused denting described above.

SAFETY PRECAUTIONS APPLIED TO DE-ICING SYSTEMS.
This section describes the safety precautions and checks and balances that should be designed into de-icing systems.

CYCLE TIMING. Contemporary de-icing systems are operated either manually, as in many general aviation aircraft, or automatically. An automatic system is one that, once activated, continues to cycle until de-activated by the pilot. A manual system cycles once per pilot activation. The most common automatically operated turbine engine inlet de-icing systems are electrothermal systems and pneumatic boots.

The most critical concern when setting the timing of a cyclical de-icer is that the ice accreted between de-icing cycles be limited to levels that can be tolerated by the engine when such ice is shed. When a cycle timer is involved, ice accretion rates must be determined for all flight regimes, and a worst-case accretion rate must be used to set the maximum allowable cycle interval.

Mechanical de-icing systems offer more flexibility than thermal systems in controlling de-icing timing cycles. Due to the operational characteristics of the anti-icing systems in large engines, ice ingestion has had to be addressed from the worst-case situation in which all potentially accreted ice is assumed to be ingested. This requirement is based on FAR Part 33.77 ("Delayed Actuation of the Anti-Ice System with Accreted Ice"). This approach may not be applicable to a de-icing system. When activated, a de-icing system only removes ice from a portion of the inlet, whereas an anti-icing system, when activated, removes ice from the entire inlet at the same time. Therefore, the amount of ice that an engine ingests in this worst-case situtation with a de-icing system is less severe than that with an anti-icing system.

Zone-by-zone de-icing of an inlet is also advantageous in designing de-icing systems that meet the ice ingestion tolerances of engines. To do this, the ice ingestion tolerance of the engine must be known, and the fragment size and amount of ice shed with a particular type of de-icer must be evaluated as to whether it falls within engine ingestion limits. The cycle interval for each zone would then be set to avoid ice accretion beyond that which can be tolerated by the engine when the ice is shed and ingested. (This is based on the worst-case ice accretion rate for a particular inlet geometry). For proprietary reasons, the ice ingestion tolerances of engines were not available for inclusion in this study.

WATER RUNBACK. Electrothermal de-icing systems need to be designed to minimise water runback. A common technique used to control water runback as well as excessive power consumption is to alternately de-ice zones within the area to be ice protected. The forward zone undergoes a de-icing cycle first and causes some water to run back into the unheated aft zone, where the water then freezes. This aft zone then undergoes a de-icing cycle to remove the now frozen runback water.

PARTICLE SEPARATORS. Many turboprop and helicopter engines are equipped with particle bypass ducting to minimise engine ingestion of ice or foreign objects. This allows longer de-icing cycle intervals than would be allowed if no particle separation were used. These engines are generally smaller and inherently more sensitive to ice ingestion than the larger high-bypass turbofan engines.

Large turbofan engines do not now and probably will not incorporate particle separators such as those now used on the small engines of helicopters and turboprops. This means that shed ice will pass directly into the engine and impact the fan, guide vanes and possibly the acoustic panels. For these engines, the de-icing cycles must be set to minimize the size and quantity of ice shed into the engine.

ICE DETECTORS. The use of ice detectors as part of an automatic, closed-loop sensing and actuator system for de-icing will affect the de-icing cycle timing. Ice detectors will actuate a de-icer only when ice is actually present, whereas a pilot would actuate a de-icer with a fixed, predetermined cycle time either when icing is only suspected or after ice has accreted to visible levels on the aircraft's exterior. Zone-by-zone de-icing using a number of ice sensors distributed around the circumference of the inlet could negate the advantage of an automatically controlled ice release system. If all detectors of the inlet simultaneously actuate de-icing of their individual zones, an excessive, potentially damaging quantity of ice could be released into the engine.

SUMMARY

Only a small percentage of engine manufacturers currently use de-icing systems. Those that do mainly use electrothermal heaters or pneumatic boots. De-icing systems will play an increased role in future aircraft turbine engine inlet ice protection. Engine manufacturers can facilitate the use of energy-efficient de-icing systems by proper attention to detail in the design, development and qualification of new propulsion systems. By defining acceptable approaches and criteria that do not adversely affect flight safety, fuel savings can be realized through the adoption of de-icing systems instead of anti-icing.

An analytical method could not be found for determining the size and amount of ice shed during de-icing of an inlet lip, but an empirical method has been identified. This method suggests that a high-speed camera be used to record the ice shedding process so that the ice fragments released from the inlet can be characterized as they exist prior to impacting any objects and breaking. This method is described in the section entitled Engine Manufacturer's Icing Experience.

An analytical method that predicts ice fragment impact locations was identified for use in determining which parts of the engine/inlet sustain damage from ice dislodged from the inlet during de-icing. The first step of this analysis is to determine the trajectories of the shed ice. For this, existing particle trajectory computer codes may be applied to predicting the paths of shed ice fragments. This trajectory analysis identifies the engine components impacted by the ice, such as acoustic liners, fan blades, engine core, and guide vanes. Parallel to or in lieu of the trajectory/impact analysis, engine service records may supply information regarding the engine components susceptible to ice damage. A search of such records resulted in several discoveries. The first is that in over 24 million flying hours, not one incident of damage to acoustic liners has been attributable to ice shed from the inlet. Nor has there been any direct ice damage to the engine compressor or outlet guide vanes, although some secondary damage to the engine core resulted from fan blade damage caused by ice. Any severe fan blade damage that occurred was at the tips of the fan blades. Severe fan blade damage is critical because it can cause engine surging. Two analytical methods were found that may predict the severity of fan blade damage caused by ice impacts. These are described in the sections entitled Ice Impact Effects on Engine Components and General Structural Analysis of Impact Dynamics.

Ice accretion rates may be determined for various icing conditions by using the computer codes discussed in the Computer Analysis of Icing and De-Icing section. Ice accretion would be controlled by matching the timing of the de-icing cycle to the rate of ice accretion. The timing of the de-icing system would be preset so the interval between de-icing cycles is short enough to keep ice accretion to a tolerable level--a level at which air inflow is not impeded and at which ice fragments released during de-icing do not damage the engine if ingested. Automatic de-icing systems could use ice detectors to sense the rate of ice accretion and match the timing of the

cycle to the icing conditions. No information is available in the open literature regarding allowable amounts of engine inlet ice accretion and any associated performance penalties.

Ice detector manufacturers report that ice detector development is now advancing from the icing advisory stage to measuring ice accretion rates and ice thicknesses; however, integrated ice sensor/de-icing systems will only occur if system reliability is ensured.

The technology surveys conducted as a part of this research effort predicted the mid-1990s as the time frame when de-icing systems may find larger-scale application. The next generation of engines, with their smaller compressors and larger diameter fans, as well as the more advanced turboprop engines will have less energy available for operating anti-icing systems. This does not mean that de-icing systems are restricted only to future applications. Several types of engines currently in service appear to be suitable for the shift from anti-icing to de-icing. Turboshaft, propfan, ducted propfan and turbojet engines are likely candidates. The motivation for this shift is the desire to conserve energy

The process of certification of de-icing systems on turbine-engine inlets is not expected to be very different from that now used for certifying any other inlet ice protection systems. The certification procedures should include: a) design/analysis phase, b) icing wind tunnel testing (using models if existing tunnels are too small for actual inlets) and c) icing flight testing. The icing wind tunnel test may be set up to simulate the actual or projected installation geometry and operating methods. This has not been required for large contemporary turbofan anti-icing systems, since new engines and nacelles are variations of existing installations with little or no change required for their anti-icing system design and operation. Due to the maturity of current anti-icing systems for large turbofans, analysis and either dry or icing flight testing has proven adequate for certification of some current transport aircraft. Until de-icing systems proposed for use in large turbofan or propfan engines reach the level of confidence felt now for current anti-icing systems, icing ground tests probably will be needed to demonstrate de-icing performance.

A diagram of the process that an inlet de-icing system could undergo to achieve certification is shown in Figure 5-1. As shown here, an emphasis is placed on the major concerns for a de-icing system: ice accretion, ice shedding and ice impact/damage. The analyses and tests (due to lack of data, new systems may need both) are set up to allow the system designer to demonstrate to the FAA that: the system functions properly, the critical design conditions are defined, and the critical design conditions can be met. The various loops within the path to certification allow the system designer to modify the system operation (if necessary) to a configuration that will ensure safe engine/aircraft operation in icing conditions.

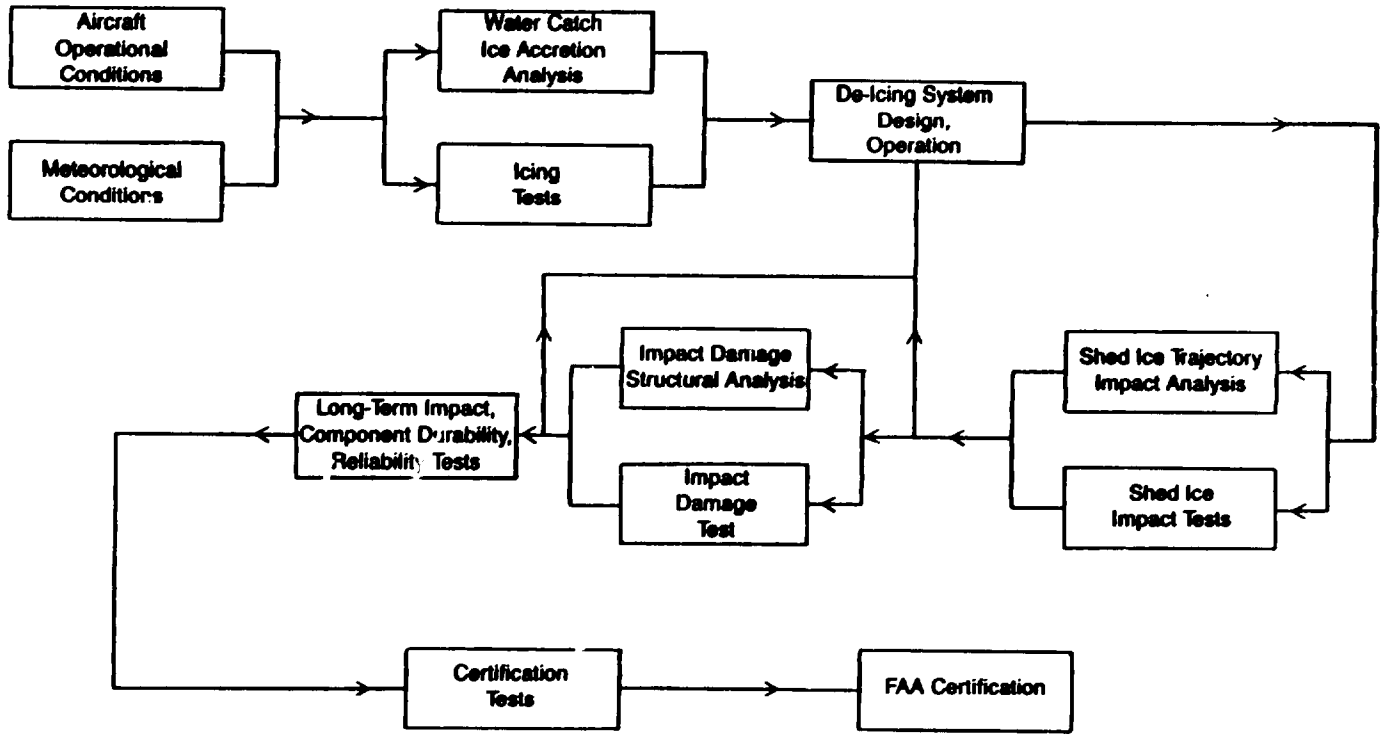

Figure 5-1. Inlet De-Ice System Certification Process

CONCLUSIONS

1. By defining acceptable approaches and criteria that do not adversely affect flight safety, fuel savings can be realized through the adoption of de-icing systems instead of anti-icing.

2. An experimental method using a high-speed camera was identified for determining the size and amount of ice shed during de-icing of an inlet lip.

3. An analytical method to predict ice fragment impact locations was identified in determining which parts of the engine/inlet sustain damage from ice dislodged from the inlet during de-icing.

4. Two analytical methods were found that may predict the severity of fan blade damage caused by ice impacts.

5. Ice accretion rates may be determined for various icing conditions by using computer codes to match the timing of the de-icing cycle to the rate of ice accretion.

6. The technology survey conducted as a part of this research effort predicted the mid-1990s as the time frame when de-icing systems may find larger-scale application.

7. The process of certification of de-icing systems on turbine engine inlets is not expected to be very different from that now used for certifying any other inlet ice protection system.

REFERENCES

DE-ICING TECHNOLOGY STATUS

2-1 Haworth, L.A., "Pneumatic Rotor Blade De-icing," VERTIFLITE, U.S. Army, September/October 1983. (Also AIAA Paper No. A83-46926).

2-2 Zumwalt, G.W. (Wichita State Universtiy) Personal Communication to H.A. Rosenthal (Rohr), October 2, 1987.

2-3 Zumwalt, G.W. and R.P. Friedberg, "Designing an Electro-Impulse De-icing System," AIAA Paper No. 86-0545, January 1986.

2-4 Zumwalt, G.W., "Electromagnetic Impulse De-icing Applied to a Nacelle Nose Lip," AIAA Paper No. 85-1118, July 1985.

2-5 Haslim, L. (NASA-Ames Research Center) Personal Communication to H.M. Rockholt (Rohr), April 7, 1988.

2-6 Nordwall, B.D., "NASA Tests Electro-Expulsive De-icer that Could Protect F/A-18 Engines," Aviation Week and Space Technology, August 3, 1987.

2-7 Rotorcraft Icing--Status and Prospects, NATO-AGARD Report No. 166, August 1981.

ICE ACCRETION AND DE-ICING EVALUATION

3-1 Lewis, G.J., "De-Icing of Aerodynamic Surfaces Using Electromechanical Impulses," Ph.D. Thesis, Nottingham University, 1985.

3-2 Macklin, W.C., USAF Contract AF 61(053)-254, Technical Report No. 9, August 1960.

3-3 Michel, B. "A Mechanical Model of Creep of Polycrystalline Ice," Canadian Geotechnical Journal, 15:1-24, 1977.

3-4 Vinogrodov, A.M. "Constitutive Modeling of Ice," Proceedings of Sixth International Off-Shore Mechanics and Arctic Engineering Symposium, Houston, Texas, March 1-6, 1987.

3-5 Sunder, S.S. and S, Nanthikesan, "A Tensile Fracture Model for Ice," Proceedings of Sixth International Off-Shore Mechanics and Arctic Engineering Symposium, Houston, Texas, March 1-6, 1987.

3-6 Reyhner, T.A., "Transonic Potential Flow Computation About Three-Dimensional Inlets, Ducts and Bodies," AIAA Journal 19:1112-1121, September 1981.

3-7 Reyhner, T.A., Computation of Transonic Potential Flow About Three-Dimensional Inlets, Ducts and Bodies, NASA CR-3514, March 1982; (Boeing Document D6-49848).

3-8 Hess, J.L. and D.M. Friedman, "Calculation of Compressible Flow In and About Three-Dimensional Inlets With and Without Auxiliary Inlets by a Higher-Order Panel Method," NACA CR-168009, October, 1982.

3-9 Maskew, B., Program VSAERO Theory Document, NASA CR-4023, September, 1987.

3-10 Magnus, E.E. and N.A. Epton, "PANAIR Computer Program for Predicting Subsonic or Supersonic Potential Flows About Arbitrary Configurations Using Higher Order Panel Method (Version 1.0), Vol. 1, Theory Document, NACA-CR 3251, 1980.

3-11 Stockman, N.O. and C.A. Farrell Jr., "Improved Computer Programs for Calculating Potential Flow in Propulsion System Inlet," NASA TM73728, July 1977.

3-12 Grashof, J., "Investigation of the Three-Dimensional Transonic Flow Around an Air Intake by a Finite Volume Method for the Euler Equations" Recent Contributions to Fluid Mechanics, ed. W. Haase, Springer-Verlag, Berlin, West Germany, 1982.

3-13 McCarthy, D.R. and T.A. Reyhner, "Multigrid Code for Three-Dimensional Transonic Potential Flow About Inlets," AIAA Journal 20:45-50, January 1982.

3-14 Papadakis, M. et al., "An Experimental Method for Measuring Droplet Impingment Efficiency on Two- and Three-Dimensional Bodies," AIAA Paper No. 86-0406, January 1986.

3-15 Breer, M.D. and W. Seibel, Particle Trajectory Computer Program User Manual, Boeing Document No. D3-0655-1, December 1974.

3-16 Kim. J.J., Particle Trajectory Computation on a 3-Dimensional Engine Inlet, NASA CR-175023, January 1986.

3-17 Norment, H.G., Calculation of Water Drop Trajectories to and about Arbitrary Three-Dimensional Lifting and Nonlifting Bodies in Potential Airflow, NASA CR-3935, October 1985.

3-18 MacArthur, C.D., "Numerical Simulation of Airfoil Ice Accretin," AIAA Paper No. 83-0112, January 1983.

3-19 Flemming, R.S. and R.J. Lednicer, "Correlation of Icing Relationships with Airfoil and Rotorcraft Icing Data," AIAA Paper No. 85-0337, January 1985.

3-20 Hoerner, S.F., Fluid Dynamic Drag, published by author, Midland Park, New Jersey, 1958.

SAFETY REQUIREMENTS SUBSTANTIATION

4-1 Hoerner, S.F., Fluid Dynamic Drag, published by author, Midland Park, New Jersey, 1958.

4-2 Wilbeck, J.S., Impact Behavior of Low-Strength Projectiles, AFML-TR-77-134, July 1973.

4-3 Barber, J.P., H.R. Taylor and J.S. Wilbeck, Bird Impact Forces and Pressures on Rigid and Compliant Targets," Technical Report AFFDL-TR-77-60, May 1978.

4-4 Boehman, L.I. and A. Challita, A Model for Prediction (sic) Bird and Ice Impact Loads on Structures, AFWAL-TR-82-2405, May 1982.

4-5 Hallquist, J.O. and D.J. Benson, DYNA3D User's Manual (Nonlinear Dynamic Analysis of Structures in Three Dimensions), UCID-19592, Rev. 2, Lawrence Livermore National Laboratory, March 1986.

CONCLUSIONS

5-1 Cohen, I.D., "Preliminary Results of the AFGL Icing Study," Air Force Geophysics Laboratory, AIAA Paper No. A83-38718, June, 1983.

5-2 Forester, G.O. and J.S. Orzechowski, "Icing and Its Measurement," A70-10692, Naval Air Propulsion Test Center, October 1969.

APPENDIX A — ICING CONDITIONS

Air contains water in the vapor phase. The maximum amount of water vapor possible in any parcel of air is dependent on the air temperature. If cooling occurs, a temperature may be reached where the air can hold no more water in the vapor state and is considered to be saturated--the relative humidity is 100 percent. Further cooling results in condensation, with the excess water vapor changing to liquid water. The water forms on condensation nuclei--minute, hygroscopic (having an affinity for water) particles suspended in the air. Sodium chloride particles from ocean spray, sulphate particles of combustion and dust particles can all act as condensation nuclei. This is the primary process for the formation of clouds, but an extremely complex process that does occasionally result in anomolies. With a high concentration of nuclei in the air, condensation can occur at relative humidities less than 100 percent. When the condensation nuclei are in low concentration or the nuclei are not hygroscopic, relative humidities in excess of 100 percent (supersaturation) can occur.

When air temperatures are above freezing, the clouds formed do not impose a threat of aircraft icing. But when condensation occurs at or below 32°F, the cloud droplets formed are termed "supercooled." It is the instantaneous or near-instantaneous freezing of these supercooled water droplets impinging on the aircraft that is the most common cause of aircraft icing.

Supercooled clouds are common, especially where temperatures are not colder than about 15°F; however, they have been found at temperatures as low as -40°F. These "colder" supercooled clouds are very unstable and can change to ice rapidly if a few ice crystals are introduced or if agitation occurs, either by atmospheric turbulence or aircraft passage. During the transition period, when the cloud is composed of both ice crystals and water droplets, it is known as a cloud of "mixed conditions."

When air temperature is appreciably below freezing, water vapor may crystallize onto nuclei as ice without ever passing through a liquid phase. Clouds thus formed consist entirely of minute, suspended ice crystals. Snow is formed of aggregates of such ice crystals that have obtained sufficient size and weight to overcome gravity, thus falling as precipitation. Flight through ice clouds or mixed condition clouds is usually not conducive to airframe icing but can be a serious icing problem for engines and engine inlets.

The type, amount and shape of accreted ice depend on: 1) atmospheric characteristics such as air temperature; liquid water content (LWC) of the cloud; and water droplet size [often referred to as MVD (median volumetric diameter)]; and 2) aircraft and flight variables such as airspeed; exposure time; and size, geometry and skin temperature of aircraft components. Other factors, such as relative humidity, solar radiation and ambient pressure at flight level, sometimes have influence, but to a lesser degree.

Rime ice forms when droplets freeze on contact with the aircraft surface and air is trapped in the ice, thus giving it a cloudy appearance. Glaze ice forms when droplets freeze while running back along the surface of the aircraft (or existing ice). This type of ice appears clear.

APPENDIX B — EIDI TESTING

TEST OF EIDI ON BUSINESS JET (FALCON-20) INLET.
A bare turbofan inlet (no engine installed) was mounted in the NASA-Lewis icing wind tunnel. Several types of EIDI coil arrangements and mounting configurations were studied (Ref. B-1). Electric power levels (voltage and capacitance) were varied (Table B-1) to determine efficiency of coil design for each mounting configuration. Efficiency was defined as the lowest level of power required to satisfactorily remove ice.

Table B-1. Electric Power Variables in EIDI Test on Business Jet Inlet

De-icing Variables					
Capacitance (μf)	200	300	400	600	
Voltage (V)	800	1000	1200	1400	1600

Initially, tests were run through the range of icing conditions shown in Table B-2, which were selected from the FAR Part 25 Appendix C icing envelope. The worst-case icing conditions were determined and used for most of the later testing. For EIDI, these conditions are warm air and light water, which produce wet and slushy ice. EIDI became effective in removing ice at thicknesses of one-eighth inch and greater.

Table B-2. Icing Condition Variables in EIDI Test on Business Jet Inlet

Icing Conditions					
Angle of Attack (deg.)	0	10			
Tunnel Air Temperature (°F)	15	27			
Tunnel Airspeed (mph)	110	170	225		
Water Droplet Diameter (μm)	12	13	15	20	
Liquid Water Content (g/m^3)	0.60	0.85	1.20	1.65	2.40

The five different types of coil-mounting methods tested are illustrated schematically in Fig. B-1. Coils were installed on the inlet lip at the numbered circumferential positions shown in Fig. B-2. Coils were tested individually and in combinations to evaluate local and interactive effects of EIDI. De-icing of an iced inlet lip could be observed visually as shown in Fig. B-2. In this case, coils at position 7 had been activated. From these performance tests, it was concluded that skin-mounted coils de-iced most efficiently (Ref. B-1). The second-most efficient arrangement was the bulkhead-mounted paired side coils.

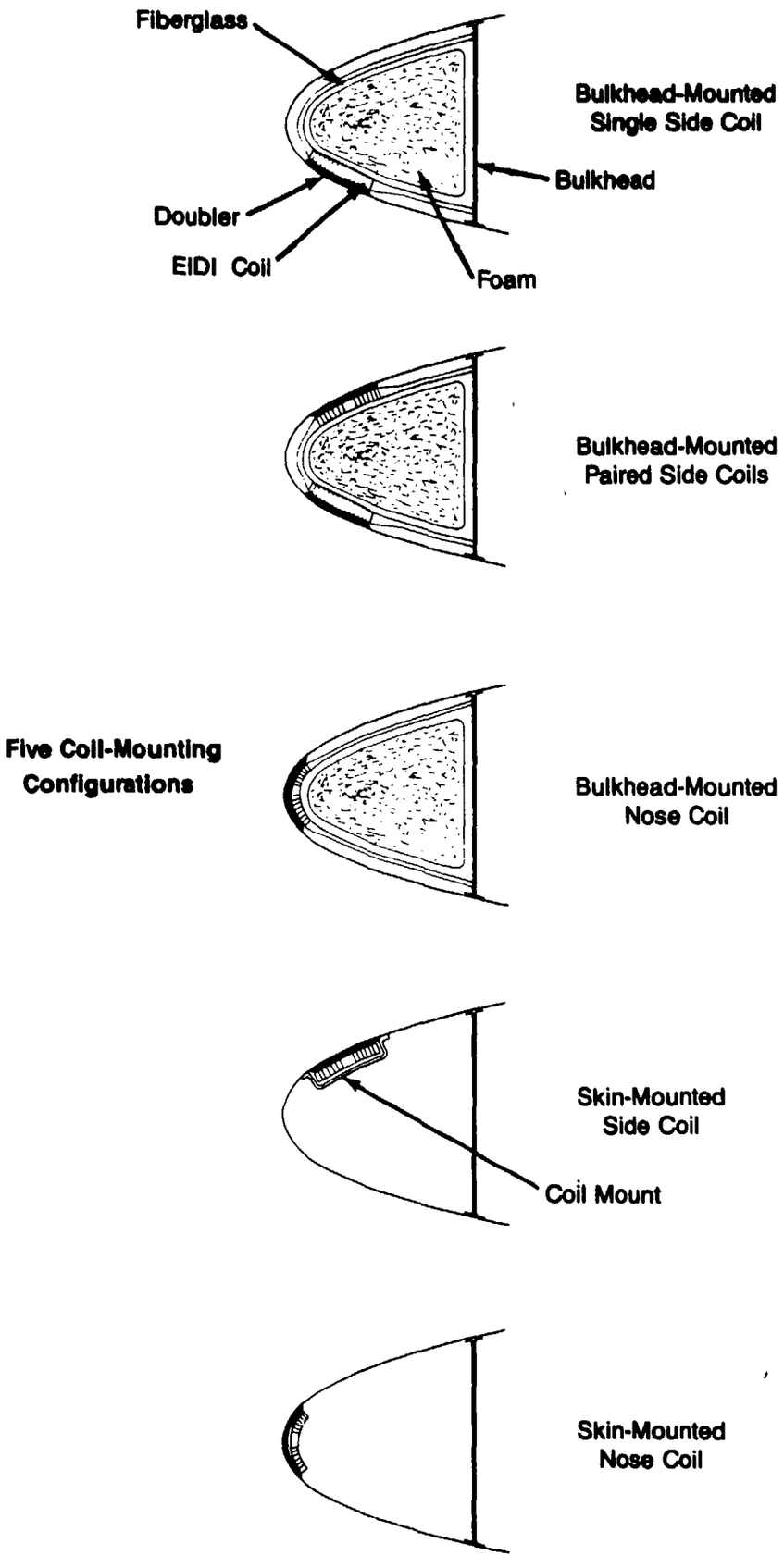

Figure B-1. EIDI Coil-Mounting Configurations—Schematic sections of an inlet lip showing different types of coil-mounting configurations tested on the business jet inlet.

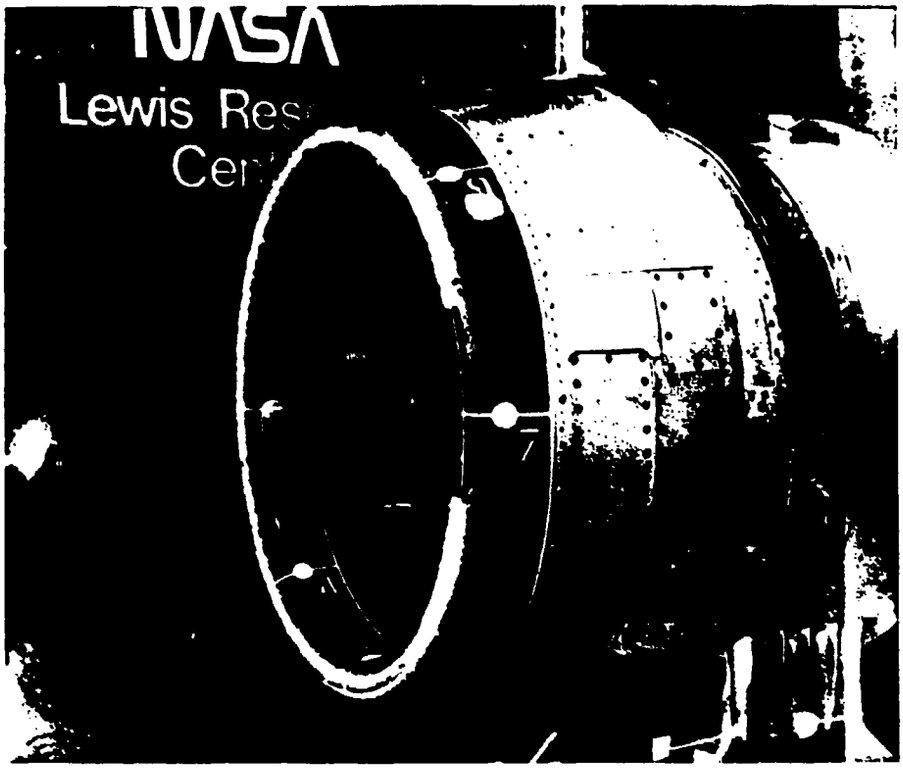

Region 7 of Inlet De-iced

- Bulkhead-Mounted Paired Side Coils
  — Positions 1, 3, 5, 7
- Nose-Mounted Paired Side coils
  — Position 4
- Skin-Mounted Nose Coil
  — Position 6
- Bulkhead-Mounted Nose Coil
  — Position 2
- Skin-Mounted Independent Side Coils
  — Positions 8, 9

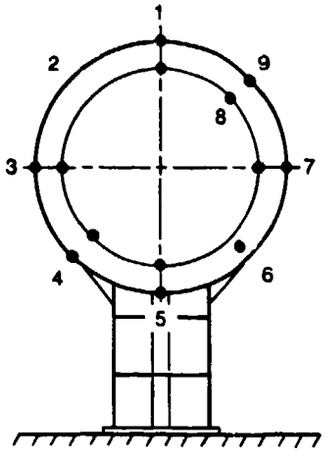

Circumferential Positions of Coils on Inlet

Figure B-2. EIDI Test—Iced business jet inlet lip has been de-iced in Region 7 by activating EIDI coils in that region during wind tunnel test.

Each of these two coil-mounting configurations was then tested over the whole circumference of an inlet lip. These tests confirmed the successful performance of the two mounting configurations during repeated de-icing cycles throughout long icing durations (30 minutes). In addition, an optimum circumferential coil spacing (the largest interval between coils that results in de-icing of the entire region) of 18 to 20 inches was determined. Based on the the business jet tests, estimates could be made of the power that would be required to effectively de-ice larger diameter inlets for turbofans. Table B-3 compares these estimates.

Shed ice fragments were caught so that their size and shape could be determined. Ice shed by EIDI in this test was one-eighth inch thick and fragment diameters were approximately three-eighths inch. This means the thickness-to-diameter aspect ratio was approximately 3:1. Further testing should be carried out to determine whether this ratio can be generalized to other ice thicknesses.

TEST OF EIDI ON TURBOPROP (PW124) INLET.

The NASA-Lewis Icing Research Tunnel was used to test EIDI on a bare inlet lip (no engine installed) designed for turboprop engine installation. Metallic doublers were bonded to the lip surfaces between the surface and each coil (as shown in Fig. B-1). This was the first test of EIDI in a composite inlet and was made in preparation for the test of EIDI on a composite turboprop inlet installed on an operating engine.

The purpose of the test was to determine the power needed for effective de-icing on a composite inlet lip. Testing conditions were similar to those of the metal business jet inlet (Ref. B-1). The composite inlet lip demonstrated good structural response, flexing and rippling during the electromagnetic impulses without breaking, but with enough displacement to expel the ice. Ice was shed effectively at electric power levels similar to those found to be effective in the business jet inlet. The thickness of ice shed was also similar for the two types of inlet.

Table B-3. Estimates of Power Required to De-Ice Different Sizes of Engine Inlets with EIDI (Bulkhead-Mounted Paired Side Coils; One-Minute Cycle On-Times)

Inlet Diameter (Feet)	Total Power (Watts)	No. Coil Stations
2.5	40	6
5.0	160	12
7.5	360	18
10.0	640	24

TEST OF EIDI ON TURBOPROP INLET ON AN OPERATING ENGINE.
EIDI was tested on the inlet of an operating turboprop engine (PW124) mounted in the Canadian National Research Council icing wind tunnel in Ottawa. The power level and timing of impulse cycles used were those determined from the previous test of the bare turboprop inlet to be the most efficient. Testing in this case was conducted similarly to FAA engine/inlet certification testing, with careful attention given to simulating FAR Part 25 Appendix C icing conditions and run durations. The inlet was equipped with a particle bypass duct, causing most, if not all, shed ice to bypass the engine, thus avoiding any concern with effects of ingested ice on the engine. EIDI performed satisfactorily for all conditions tested. Low-temperature conditions (0°F to -22°F) were not tested, due to the environmental constraints of the facility. However, the results of the NASA-Lewis tests had already demonstrated that EIDI performs best in this low-temperature range.

Based on the two turboprop tests, EIDI appears to be a good candidate for ice protection on turboprop engine inlets, provided other considerations such as reliability, maintainability, resistance to fatigue, and cost are acceptable.

TEST OF EIDI ON LARGE DIAMETER (A310) TURBOFAN INLET.
A one-quarter span of a large (eight-foot diameter) turbofan inlet was mounted in France's Centre D'Essais Des Propulseurs R-2 icing wind tunnel (Fig. B-3). A four-foot diameter uniform icing cloud was produced, which exposed a 75- to 80-degree span of the inlet to icing. Six EIDI coil stations were equally spaced over the span of the inlet, approximately one foot apart, with two coils per station. Testing conditions again reflected the FAR Part 25 Appendix C icing envelope. The results of this test provided information about large diameter inlet configurations. The minimum ice thickness at which EIDI became effective was the same as in previous tests--one-eighth inch.

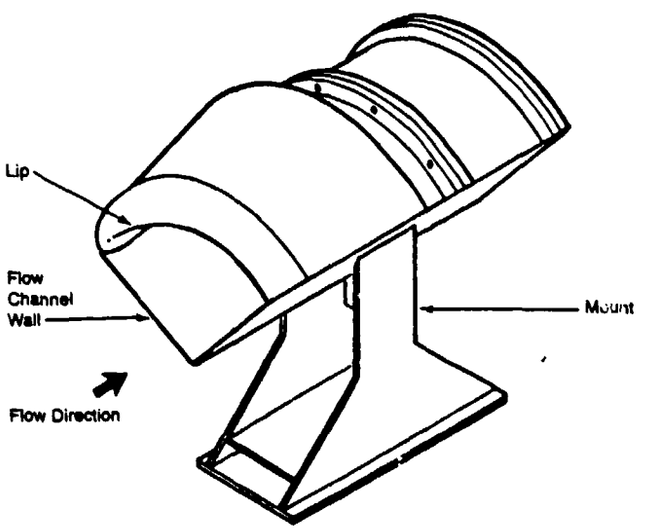

Figure B-3. One-Quarter Section of Turbofan Inlet as Mounted for Testing in Icing Tunnel

Excellent viewing of shed ice was accomplished by filming many de-icing cycles at 1,000 and 4,000 frames per second. This data was edited into videotape format and analyzed to determine ice particle size, shape and shedding trajectory. Ice particles shed from the larger (A310) turbofan inlet had a higher diameter-to-thickness ratio (10:1) than ice particles shed from the smaller inlets of business jet and turboprop engines, which have a 3:1 ratio.

SKIN FATIGUE TESTS.
An EIDI system relies on deformation of the aircraft skin for its operation; therefore, it subjects the skin to stress. Consequently, fatigue resistance of the structure must be considered.

Fatigue tests of two light Cessna general aviation airplane wings were conducted at Wichita State University. Using environmental temperatures and de-icing power levels similar to those in previous tests, no structural damage to the wings was apparent after 15,000 EIDI de-icing impulses. A composite leading edge was similarly tested for 20,000 cycles with no structural damage. In fatigue studies of a large transport aircraft wing slat at much higher voltages (3,000 volts), the wing slat withstood 69,000 impulses before showing signs of fatigue (cracks in the skin). Thus, fatigue does not appear to be a concern. However, given the complexity of the task of analyzing the dynamic response (i.e., vibrational modes) of a realistic structure to an EIDI impulse and predicting accurate structural stresses, a fatigue test of any new EIDI installation should be carried out.

TEST OF EIDI ON A FULL-SIZE ENGINE INLET.
An EIDI system was tested on a full-size engine inlet in the Rolls-Royce Hucknall icing wind tunnel. The purpose of these tests was to demonstrate EIDI's performance over a range of atmospheric icing conditions (temperature = -5°C, -10°C , -20°C; LWC = 0.6g/cm^3; airspeed = 253 fps; droplet size = 20 microns). A high LWC was selected to achieve a high rate of ice accretion between pulses, thereby decreasing time required for the testing. The test temperature range produced both rime and glaze ice. No tests were carried out in simulated ice crystal conditions. These tests revealed the following aspects of EIDI that will require attention during the design stage.

AIRCRAFT STRUCTURE INFLUENCES WAVE PROPAGATION. The principle of operation of EIDI is to set up mechanical disturbances in the aircraft skin to be de-iced. The magnitude of the disturbance decays with time and distance from the coil. If there is sufficient distance between structural supports of the aircraft skin (such as spars or ribs), waves originating in the skin over the coil may travel relatively long distances in the skin until they dampen out naturally. If the intervals between skin supports are less than 10 coil diameters spanwise or less than five diameters chordwise, waves are reflected from the supports and are of relatively large amplitude compared with the original disturbance. Constructive interference can result, setting up standing waves in the skin, thereby improving the efficiency of the system.

Actual EIDI installations tend to be a combination of these circumstances. In the chordwise direction, both wing leading edges and engine inlet lips have skin supports close to the coils. Standing waves can be set up in this direction, and therefore, coil size and positioning become important for good de-icing performance. Coils that are poorly positioned or coils that are too big compared to the distance between structural nodes will cause destructive interference of the induced waves, resulting in low amplitude displacements and, thus, reduced EIDI efficiency.

Spanwise wave propagation may differ greatly from chordwise propagation. If no ribs are present in a wing, traveling waves are not reflected but decay naturally. Similarly, most engines have inlet cowls supported only at the rear. Coil positioning in the circumferential direction is not critical for good pulse propagation, but circumferential spacing must be addressed for effective de-icing between coils.

ELECTRICAL DESIGN. EIDI works on the principle of electromagnetic induction. For best results, the aircraft skin adjacent to the EIDI coil should be non-magnetic and have high electrical conductivity. EIDI has been used with composite aircraft skins by means of attaching a metal plate (a doubler) (Fig. B-1) to the skin adjacent to the coil.

Due to the high electrical currents passing through the coils of an EIDI system, connecting wires will repel each other. They will also be repelled by any metallic structures close to them. The forces involved are relatively small but are sufficient to move the wires if they are not secured at frequent intervals. Chafing of insulation and fatigue fracture of cables at their connecting points have been noted by some EIDI researchers. These problems can be resolved provided they are recognized early in the design stage.

Another important factor relating to the design of the EIDI system is lightning strike resistance. Lightning striking the engine inlet or wing leading edge must be provided with a low-resistance path back to the main aircraft structure in order for it to dissipate harmlessly. If this path is not provided, a lightning strike could provide very high voltage into the EIDI system and destroy it.

COIL-MOUNTING BRACKETS. The coil-mounting brackets are subjected to the same load as the aircraft skin. This may be as high as 900 lbs. (4KN) per impulse over the coil area. Each impulse lasts approximately 0.5 to 1.0 millisecond. The mounting brackets must be designed for these loads. A major purpose of the mounting bracket is to maintain the correct coil-to-skin gap. The brackets should limit deflection of the coil during an impulse to 0.010 inch (0.25 mm) or less to prevent the coil and skin from coming into contact.

The coil brackets should not affect the magnetic field produced by the EIDI coil. Materials which are non-magnetic and non-conducting should be used. For example, glass fiber composites are preferred over electrically conducting carbon fiber.

STRUCTURAL DYNAMICS.
Since EIDI removes accreted ice by a process which applies localized rapid accelerations to aircraft surfaces, it was realized that structural dynamics analysis was a necessary design and development tool. However, for an optimum structural dynamics analysis, it is necessary to specify the force-versus-time (forcing function) that an EIDI system imparts to the structure.

Wichita State University (WSU) and NASA developed an electrodynamic analysis computer code that serves this purpose. Based on EIDI system physical parameters such as coil size, spacing, voltage, capacitance, inductance, and wire resistance, the code calculates electrical response of the system and outputs a force-versus-time function (Ref. B-2). This function can serve as the input for the structural dynamics analysis.

WSU also developed a structural dynamics model that produces an output consisting of a set of natural frequencies, vibrational mode shapes, accelerations displacements and stresses. These calculated stresses and displacements were compared to data from structural response tests of actual hardware conducted at WSU. The analysis results correlated well with the test data.

With such a structural dynamics model, numerous design iterations can be produced to: (1) evaluate materials; (2) determine optimal locations for EIDI inductor coils; (3) determine impulse response of the aircraft skin; and (4) predict loads imparted in local aircraft structure and associated mounting hardware. The loads and structural responses would then be used to predict fatigue life.

EIDI ENERGY CONSUMPTION.
The amount of energy required to remove accreted ice from a surface using an EIDI system is calculated below and compared to the amount of energy required for other types of ice protection. As evident from these figures, electromagnetic impulse de-icing is much more energy-efficient than either evaporative anti-icing or thermal methods of melting ice.

EIDI tests have indicated that two impulses per coil station are required to remove accreted ice.

The energy consumed per impulse (E_i) is:
$E_i = 0.5CV^2 = 200$ joules
(where C = 400 microfarads and V = 1,000 volts).

The energy consumed per coil station (E_s) is:
$E_s = 2E_i = 400$ joules = 0.38 BTUs.

This amount of energy will remove a 0.1"-thick layer of ice over an 18" x 6" area.

The mass of ice removed = (ice density) x (ice volume)
$= (0.0325\ lb/in^3) \times (18"x6"x0.1") = 0.35$ lb.

The energy required for EIDI = 0.38 BTU/0.35 lb = 1 BTU/lb.

In comparison:

Task	Energy Required (BTU/lb)
Evaporate Water	1,000*
Melt Ice	144*
Remove Ice with EIDI	1

*Additional energy is needed above these values for thermal systems because of heat losses.

APPENDIX B REFERENCES

B-1 Nelepovitz, D.O. and H.A. Rosenthal, "Electro-Impulse De-icing of Aircraft Engine Inlets," AIAA Paper No. 85-0546, January 1986.

B-2 Bernhart, W.D. and R.L. Schrag, "Electro-Impulse De-Icing Electrodynamic Solution by Discrete Elements," AIAA Paper No. 88-0018, January 1988.

APPENDIX C — DISTRIBUTION LIST

Recipient	No. Copies
ATA of America Attn: Dick Tobiason 1709 New York Avenue, NW Washington, DC 20006	1
Bocing Commercial Airplane Co. Attn: Walt Bauermeister, MS 9W-60 P.O. Box 3707 Seattle, WA 98124-3707	1
Boeing Commercial Airplane Co. Attn: Doug Cosby P.O. Box 3707 Seattle, WA 98124-3707	1
Boeing Commercial Airplane Co. Attn: Derek Rouse, MS 6L-65 P.O. Box 3707 Seattle, WA 98124-3707	1
Boeing-Vertol Company Attn: Andy Peterson, MS 32-16 P.O. Box 16858 Philadelphia, PA 19142	1
British Embassy Civil Air Attache ATS 3100 Mass Ave., NW Washington, DC 20008	1
Civil Aviation Authority Aviation House 129 Kingsway London WC2B 6NN, England	1
Continuum Dynamics, Inc. Attn: Dr. Alan Bilanin P.O. Box 3073 Princeton, NJ 08543	1
Director DuCentre Exp de la Naviation Aerineene 941 Orly, France	1
DOT/FAA AEU-500 American Embassy, APO New York, NY 09667	4
DOT/FAA Central Region ACE-66 601 East 12th Street Federal Building Kansas City, MO 64106	1
DOT/FAA Great Lakes Region AGL-60 O'Hare Office Center 2300 East Devon Avenue Des Plaines, IL 60018	2
DOT/FAA National Headquarters ADL-1 800 Independence Avenue, SW Washington, DC 20591	2
DOT/FAA National Headquarters ADM-1 800 Independence Avenue, SW Washington, DC 20591	2
DOT/FAA National Headquarters ALG-300 800 Independence Avenue, SW Washington, DC 20591	2
DOT/FAA National Headquarters APA-300 800 Independence Avenue, SW Washington, DC 20591	2
DOT/FAA National Headquarters ASF-1 800 Independence Avenue, SW Washington, DC 20591	2
DOT/FAA National Headquarters ASF-100 800 Independence Avenue, SW Washington, DC 20591	2
DOT/FAA National Headquarters ASF-200 800 Independence Avenue, SW Washington, DC 20591	2

Recipient	No. Copies
DOT/FAA National Headquarters ASF-300 800 Independence Avenue, SW Washington, DC 20591	2
DOT/FAA National Headquarters AVS-1 800 Independence Avenue, SW Washington, DC 20591	2
DOT/FAA National Headquarters AVS-100 800 Independence Avenue, SW Washington, DC 20591	2
DOT/FAA National Headquarters AVS-200 800 Independence Avenue, SW Washington, DC 20591	2
DOT/FAA National Headquarters AVS-300 800 Independence Avenue, SW Washington, DC 20591	2
DOT/FAA National Headquarters AWS-1 800 Independence Avenue,SW Washington, DC 20591	2
DOT/FAA Mike Monroney Aeronautical Center AAC-64D P.O. Box 25082 Oklahoma City, OK 73125	2
DOT/FAA Southwest Region ASW-53B P.O. Box 1689 Fort Worth, TX 76101	2
Embassy of Australia Civil Air Attache 1601 Mass. Ave., NW Washington, DC 20036	1
FAA, Chief Civil Aviation Assistance Group Madrid, Spain American Embassy, APO New York, NY 09285-0001	1
FAA Anchorage ACO 701 C Street, Box 14 Anchorage, AK 99513	1
FAA Atlanta ACO 1075 Inner Loop Road College Park, GA 30337	1
FAA Boston ACO 12 New England Executive Park Burlington, MA 001803	1
FAA Brussels ACO American Embassy, APO New York, NY 09667	1
FAA Denver 10455 East 25th Avenue Suite 307 Aurora, CO 98168	1
FAA Long Beach ACO 4344 Donald Douglas Drive Long Beach, CA 90808	1
FAA Los Angeles ACO P.O. Box 92007 Worldway Postal Center Hawthorne, CA 90009	1
FAA New York ACO 181 So. Frankline Ave., Rm 202 Valley Stream, NY 11581	1
FAA Seattle ACO Attn: Mark Quam 17900 Pacific Highway So. C-68966 Seattle, WA 98168	1
FAA Wichita ACO Mid-Continent Airport Room 100 FAA Building 1891 Airport Road Wichita, KS	1
General Electric Company Attn: Dick Keller Aircraft Engine Group Cincinnati, OH 45215	1

Recipient	No. Copies
McAir Propulsion Systems Attn: A.M. Espinosa, MS 425 St. Louis, MO 63136	1
Naval Air Propulsion Center P.O. Box 7176 Trenton, NJ 08628	1
Naval Air Test Center Attn: Brion Picard Flight Systems Dept. Patuxent River, MD 20670	1
Northwestern University Trisnet Repository Transportation Center Library Evanston, IL 60201	1
Scientific & Tech. Info FAC Attn: NASA Rep. P.O. Box 8757 BWI Airport Baltimore, MD 21240	1
Sverdrup Technology, Inc. Attn: Dr. J.D. Hunt, T-327 NSTL, MS 39529	1
Sverdrup Technology, Inc. Attn: Tom Miller Box 30650 Middleberg Heights, OH 44130-9998	1
University of California Service Dept. Institute of Transportation Standard Lib 412 McLaughlin Hall Berkely, CA 94720	1
University of Michigan Attn: Gary Ruff Dept. of Aerospace Ann Arbor, MI 48104	1
USAF Aeronautical Systems Division Attn: Steve Johnson ASD-WE Wright-Patterson Air Force Base, OH 45433-6503	1

Recipient	No. Copies
USAF Flight Test Center Attn: Kelly Adams G520 Test Group/ENAS 239 Edwards Air Force Base, CA 93532	1
Mr. Richard Adams National Resource Specialist AWS-104 FAA 800 Independence Avenue, SW Washington, DC 20591	2
Mr. Al Astorga FAA (CAAG) American Embassy, Box 38, APO New York, NY 09285-0001	1
Mr. C. Scott Bartlett Sverdrup Technology, Inc. USAF Arnold Engineering Development Center Arnold Air Force Station, TN 37389	1
Mr. Gale Braden FAA 5928 Queenston St. Springfield, VA 22152	1
Mr. Burton Chesterfield, DMA-603 DOT Transportation Safety Inst. 6500 South McArthur Blvd. Oklahoma City, OK 73125	1
Mr. Gary Frings Flight Safety Research Branch ACT-340 FAA Technical Center Atlantic City International Airport, NJ 08405	50
Mr. Bill Gaitskill U.S. Army Aviation Systems Command 4300 Goodfellow Boulevard AMSAV-ED St. Louis, MO 63120	1
Dr. John Hansman Massachusetts Institute of Technology Department of Aeronautics Cambridge, MA 02139	1

Recipient	No. Copies
Mr. Paul Hawkins Propulsion Branch, ANM-140S FAA 17900 Pacific Highway South C-68966 Seattle, WA 98168	1
Mr. Robert Koenig Engine and Propeller Standards Staff, AME-110 FAA 12 New England Executive Park Burlington, MA 01803	1
Dr. Kenneth Korkin Texas A&M University Department of Aeronautical Engineering College Station, TX 77840	1
Dr. Hans A. Krakauer Deputy Chairman International Airline Pilots Association Group Apartado 97 8200 Albufeira, Portugal	1
Mr. Geoffrey Lipman Executive Director, President du Conseil International Foundation of Airline Passenger Associations Case Postale 462, 1215 Geneve 15 Aeroport, Swisse, Geneva	1
Mr. Richard E. Livingston Jr. Director, Aerotech Operations for the IAPA Group 1805 Crystal Drive Suite 1112 South Arlington, VA 22202	1
Mr. Byron Phillips National Center for Atmospheric Research Research Aviation Facility P.O. Box 3000 Boulder, CO 80307	1
Dr. Joe Shaw NASA-Lewis Research Center 21000 Brookpark Road Mail Stop 86-7 Cleveland, OH 44126	1

Recipient	No. Copies
Mr. Frank Taylor 3542 Church Road Ellicott City, MD 21403	1
Mr. William T. Westfield Manager, Engine/Fuel Safety Branch, ACT-320 FAA Technical Center Atlantic City International Airport, NJ 08405	1
AAC-64D	2
AAL-400	2
ACE-66	2
ACT-5	2
ACT-61A	2
ADL-1	1
ADL-32 North	1
AEA-61	3
AES-3	1
AGL-60	2
ALG-3900	1
ANE-40	2
ANM-60	2
APA-300	1
APM-1	1
APM-13 Nigro	2
ASO-52C4	2
ASW-53B	2
AWS-100	1
M-493.2	5